

Supporting Information

Highly Dispersed Silica-Supported Iridium and Iridium-Aluminium Catalysts for Methane Activation Prepared via Surface Organometallic Chemistry

Léon Escomel,^a Daniel F. Abbott,^b Victor Mougel,^b Laurent Veyre,^a Chloé Thieuleux^a and Clément Camp^{*a}

[a] Laboratory of Chemistry, Catalysis, Polymers and Processes, C2P2 UMR 5265, Université de Lyon, Institut de Chimie de Lyon, CNRS, Université Lyon 1, ESCPE Lyon, 43 Bd du 11 Novembre 1918, F-69616 Villeurbanne, France.

[b] Laboratorium für Anorganische Chemie, ETH Zürich, Vladimir-Prelog-Weg 1, CH-8093 Zürich, Switzerland

Content

A. Experimental section.....	2
A.1 General considerations	2
A.2 Characterisation methods.....	2
A.3 Syntheses	3
B. NMR spectroscopy data	6
C. IR spectroscopy data	10
D. X-ray crystallography	11
E. X-ray photoelectron spectroscopy (XPS) data.....	13
F. STEM-HAADF micrographs and EDX data.....	16
G. H ₂ Chemisorption studies	21
G.1 H ₂ Chemisorption isotherms.....	21
G.2 Calculation of the dispersion and NPs size	21
H. Catalysis	22
H.1 Procedure.....	22
H.2 Kinetic graphs.....	23
H.3 Mechanistic considerations	27
I. Authors contributions and acknowledgements	29
J. References.....	29

A. Experimental section

A.1 General considerations

Unless otherwise noted, all reactions were performed either using standard Schlenk line techniques or in an MBraun inert atmosphere glovebox under an atmosphere of purified argon (<1 ppm O₂/H₂O). Glassware and cannulae were stored in an oven at ~100 °C for at least 12 h prior to use. *n*-pentane was purified by passage through a column of activated alumina, dried over Na/benzophenone, vacuum-transferred to a storage flask and freeze-pump-thaw degassed prior to use. Deuterated solvents were dried over Na/benzophenone vacuum-transferred to a storage flask and freeze-pump-thaw degassed prior to use. Complex **1**^[1] and Cp*IrH₄^[2] were prepared using literature procedures. The SBA-15 mesoporous silica was synthesized^[3] and dehydroxylated^[4] at 700°C according to the reported procedures. All other reagents were acquired from commercial sources and used as received. D₂, H₂ and CH₄ gases were dried and deoxygenated over freshly regenerated R311G BASF catalyst/molecular sieves (4Å) prior to use. For the synthesis and treatment of surface species, reactions were carried out using high-vacuum lines (10⁻⁵ mBar) and glovebox techniques.

A.2 Characterisation methods

IR spectroscopy

Samples were prepared in a glovebox, sealed under argon in a DRIFT cell equipped with KBr windows and analyzed on a Nicolet 6700 FT-IR spectrometer.

STEM-HAADF and EDS

Electron microscopy experiments were used to understand the structural and morphological characteristics of the catalysts by using a MET JEOL 2100F (FEG) microscope at the “Centre Technologiques des Micro-structures”, CTμ Villeurbanne, France; equipped with an Oxford Instruments Energy-Dispersive Spectroscopy (EDS) SDD detector. The samples were transferred to the microscope apparatus under inert atmosphere.

Elemental analyses

ICP-MS analyses were performed under inert atmosphere at Mikroanalytisches Labor Pascher, Germany.

X-ray structural determinations

Experimental details regarding XRD measurements are provided below. CCDC 2149676 contains the supplementary crystallographic data for this paper. These data are provided free of charge by the Cambridge Crystallographic Data Centre.

NMR Spectroscopy

Solution NMR spectra were recorded on a Bruker AV-500 spectrometer. Chemical shifts were measured relative to residual solvent peaks, which were assigned relative to an external TMS standard set at 0.00 ppm. ^1H and ^{13}C NMR assignments were confirmed by ^1H - ^1H COSY and ^1H - ^{13}C HSQC and HMBC experiments. The 1D ^1H and ^{13}C solid-state NMR spectra were obtained on a Bruker 300 MHz wide-bore spectrometer using a double resonance 4-mm MAS probe. The samples were introduced under argon in a zirconia rotor, which was then tightly closed. Dry nitrogen gas was used to spin the samples to avoid sample degradation. The ^{13}C spectra were obtained from cross polarization (CP) from protons using a linear ramped CP to optimize the magnetization transfer efficiency. A proton radio frequency (RF) field of 70 kHz in the center of the ramp was applied, while the RF field on carbon-13 was adjusted for optimal sensitivity.

Chemisorption of H_2

Chemisorption experiments were performed on a Belsorb-Max apparatus from BEL Japan. In a measuring cell, 32 mg of Ir-Al/SiO_2 and 43 mg of Ir/SiO_2 were treated at 10^{-6} mbar at 523 K for 3 h using a ramp of $5 \text{ K}\cdot\text{min}^{-1}$. After this pretreatment, adsorption isotherms were measured at 298 K in the pressure range of [30-265 mbars]. In this study, we quantify the total adsorption, *i.e.* adsorption on fully degassed nanoparticles. For each experimental points, the pressures at equilibrium were recorded after a time of one hour. The quantification of gas adsorbed on surface metal atoms was calculated from the adsorption at saturation deriving from a double Langmuir adsorption equation model, assuming complete reduction of the metal and truncated cubic octahedron geometry.

A.3 Syntheses

Synthesis of $[\text{Al}(\text{OAr})(\text{Cp}^*\text{IrH}_3)_2]$ (Ar = 2,6-(*i*Pr) C_6H_3), compound **2-m**.

A 1 mL colorless pentane solution of 2,6-diisopropylphenol (26.4 mg, 0.15 mmol, 1.0 eq.) was added dropwise into a 3.5 mL colorless pentane solution of **1** (151.0 mg, 0.15 mmol, 1.0 eq.). The resulting solution was stirred at RT for 90 minutes. Then, volatiles were removed in *vacuo* yielding white solids (c.a. 170 mg). The latter was dissolved in the minimum amount of pentane (c.a. 8 mL), filtered, and cooled to -40°C for 24 hours yielding compound **2-m** as colorless needle-shaped crystals (100 mg, 77% yield). ^1H NMR (400 MHz, 293K, C_6D_6) δ 7.21 (d, $^3J_{\text{HH}}=7.5$ Hz, 2H, $\text{CH}_{\text{Ar-meta}}$), 7.00 (t, $^3J_{\text{HH}}=7.6$ Hz, 1H, $\text{CH}_{\text{Ar-para}}$), 3.75 (m, 2H, CH_{IPr}), 1.98 (s, 30H, Cp^*), 1.47 (d, $^3J_{\text{HH}}=6.8$ Hz, 12H, $\text{CH}_3\text{-iPr}$), -16.55 (s, 6H, Ir-H). $^{13}\text{C}\{^1\text{H}\}$ NMR (75 MHz, 293K, C_6D_6) δ 154.83 ($\text{C}_{\text{Ar-O}}$), 137.10 ($\text{C}_{\text{Ar-ortho}}$), 123.38 ($\text{CH}_{\text{Ar-meta}}$), 119.24 ($\text{CH}_{\text{Ar-para}}$), 94.64 (C_{Cp^*}), 27.65 (CH_{IPr}), 24.49 ($\text{CH}_3\text{-iPr}$), 11.10 ($\text{CH}_3\text{-Cp}^*$). DRIFT (293K, cm^{-1}) σ 2962 (s, $\nu_{\text{C-H}}$), 2915 (s, $\nu_{\text{C-H}}$), 2866 (s, $\nu_{\text{C-H}}$), 2139 (s, $\nu_{\text{M-H}}$), 1998 (s, $\nu_{\text{M-H}}$), 1456 (m), 1381 (m), 1333 (m), 1277 (m). Elemental analysis calcd (%) for $\text{C}_{32}\text{H}_{53}\text{OAlIr}_2$: C 44.42, H 6.17; found: C 44.69, H 6.21.

Preparation of $[(\equiv\text{SiO})\text{Al}(\text{Cp}^*\text{IrH}_3)_2]$, material **2-s**

SBA-15₇₀₀ (340 mg dehydroxylated at 700°C under 10⁻⁵ mBar vacuum for 18 hours, 0.22 mmol of OH, 1.0 eq.) is charged in one compartment of a two-sided Schlenk reaction vessel equipped with a sintered glass filter. On the other compartment, a 20 mL dried pentane solution of complex $[\text{Al}\{\{\text{H}\}(\mu\text{-H})_2\text{IrCp}^*\}_3]$, **1** (280 mg, 0.27 mmol, 1.2 eq.) is introduced. In the glovebox, the double-Schlenk vessel is smoothly and rapidly evacuated (10⁻² mbar for a few seconds, while the pentane solution of **1** is stirred). The colorless solution of complex **1** is then transferred through the frit to the SBA-15₇₀₀ powder and stirred at room temperature for 2 h. After the reaction, the colorless supernatant is filtered away from the solid. The solid is washed with fresh pentane and the supernatant is removed again. This procedure is repeated four times to ensure removal of any unreacted **1** as well as Cp*IrH₄, which is formed as coproduct. Afterwards, pentane volatiles are gently removed *in vacuo* (10⁻² mbar for about 15 minutes, over stirring) since Cp*IrH₄ can be subjected to sublimation. This procedure affords 120 mg of a white solid containing a mixture of IrCp*IrH₄ (0.21 mmol, 1 eq./OH) and unreacted **1** (0.05 mmol, 0.2 eq.) in the first reaction vessel compartment (content analyzed by ¹H-NMR spectroscopy in C₆D₆) and 460 mg of **2-s** a white solid in the second chamber, after drying it over high vacuum (10⁻⁵ mBar) for 2 hours at room temperature. ¹H MAS SSNMR (300 MHz, 293 K) δ 1.95 (Cp*), -17.14 (Ir-H). ¹³C CP-MAS SSNMR (126 MHz, 293 K) δ 94.39 (C_{Cp*}), 9.51 (CH_{3-Cp*}). DRIFT (293K, cm⁻¹) σ 2989 (m, $\nu_{\text{C-H}}$), 2964 (s, $\nu_{\text{C-H}}$), 2913 (s, $\nu_{\text{C-H}}$), 2131 (s, $\nu_{\text{M-H}}$), 2000 (s, $\nu_{\text{M-H}}$), 1468 (m), 1388 (w). Elemental analysis calcd (%) for **2-s**: C 10.62, H 1.60, Ir 17.00, Al 1.19; found: C 10.87, H 1.69, Ir 16.40, Al 1.21.

Synthesis of material Ir-Al/SiO₂

2-s (230 mg, 0.2 mmol/Ir) was charged under argon in a 300 mL glass reactor that was evacuated under high vacuum (10⁻⁵ mbar). Then, excess of dry hydrogen gas (1036 mbar, 12.8 mmol) was introduced in the reactor. The system was heated at 250°C for about 48 hours before hydrogen was removed under high vacuum. The resulting material was dried for 30 minutes under high vacuum at 250°C. The system was then transferred in the glovebox and 195 mg of Ir-Al/SiO₂ was recovered as a brown powder. DRIFT (293K, cm⁻¹) σ 3748 (m, $\nu_{\text{SiO-H}}$), 2011 (s, $\nu_{\text{M-H}}$). Elemental analysis found for Ir-Al/SiO₂ (% wt): C 0.69, H 0.24, Ir 16.70, Al 1.22.

Incipient wetness impregnation of Cp*IrH₄ on SBA-15₇₀₀

A 0.34 mL THF colorless solution of Cp*IrH₄ (140 mg, 0.42 mmol, concentration was adjusted to achieve the desired metal loading of material **2-s**) was added dropwise onto SBA-15₇₀₀ (295 mg) to achieve incipient wetness impregnation under argon atmosphere and with vigorous stirring (using a glass spatula) to ensure homogeneous repartition of the precursor upon the support. The resulting white powder was dried *in vacuo* while stirring for 10 minutes yielding Cp*IrH₄/SiO₂ as a fine white powder.

DRIFT (293K, cm^{-1}) σ 3450 (br and w, $\nu_{\text{SiO-H}}$, umbrella effect), 2150 (s, $\nu_{\text{M-H}}$). Elemental analysis found for **IrCp*H₄/SiO₂** (% wt): C 11.80, H 1.92, Ir 16.30.

Synthesis of material Ir/SiO₂

Cp*IrH₄@SiO₂ (350 mg, 0.3 mmol/Ir) was charged in a 300 mL glass reactor. Then, argon was evacuated on a high vacuum line (until reaching a pressure of about $2 \cdot 10^{-3}$ mbar from which point Cp*IrH₄ can start to sublime). Then dry hydrogen gas (1044 mbars, 12.9 mmol) was added in the system. The reactor was heated at 250°C for 48 hours before hydrogen was removed under high vacuum. The resulting material was dried for 30 minutes under high vacuum at 250°C. Then the system was transferred in the glovebox and 300 mg of **Ir/SiO₂** was recovered as a dark brown powder. DRIFT (293K, cm^{-1}) σ 3748 (s, $\nu_{\text{SiO-H}}$), 2024 (s, $\nu_{\text{M-H}}$). Elemental analysis found for **Ir/SiO₂** (% wt): C 1.04, H 0.22, Ir 18.80.

B. NMR spectroscopy data

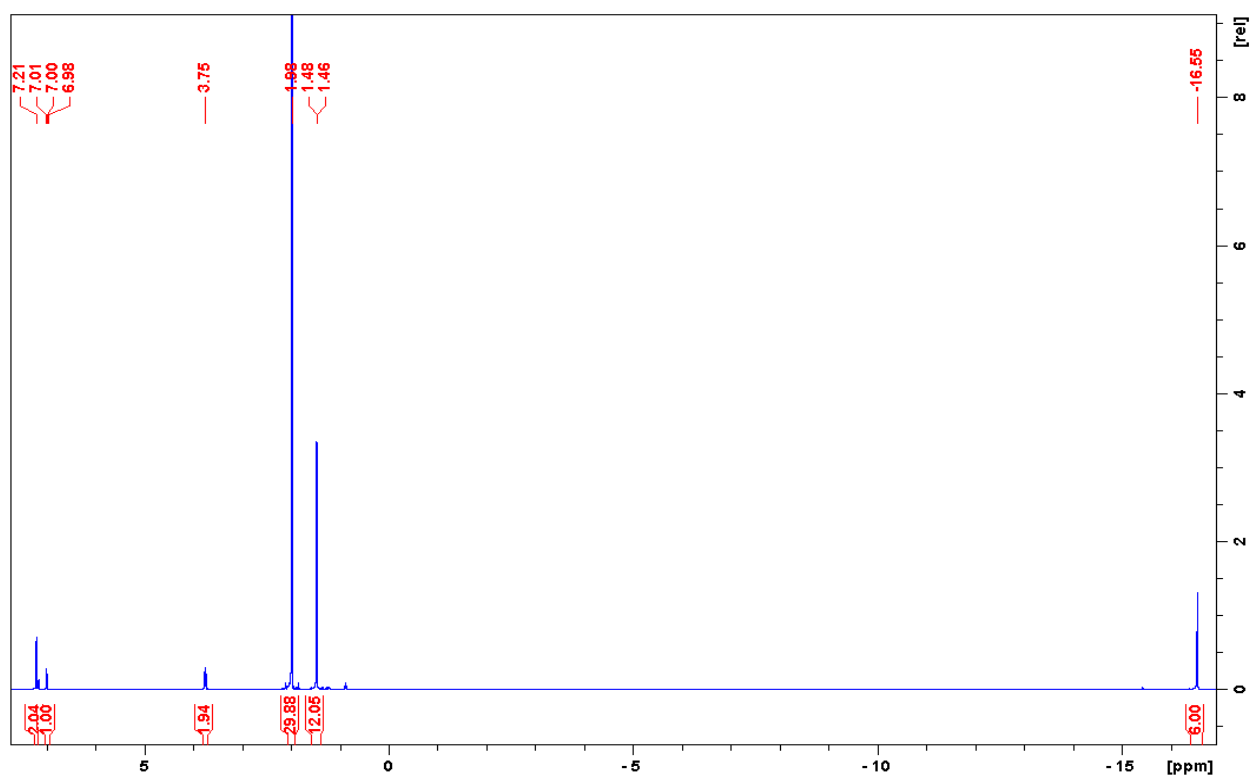


Figure S1. ¹H-NMR spectrum (500 MHz, C₆D₆, 293K) of compound 2-m.

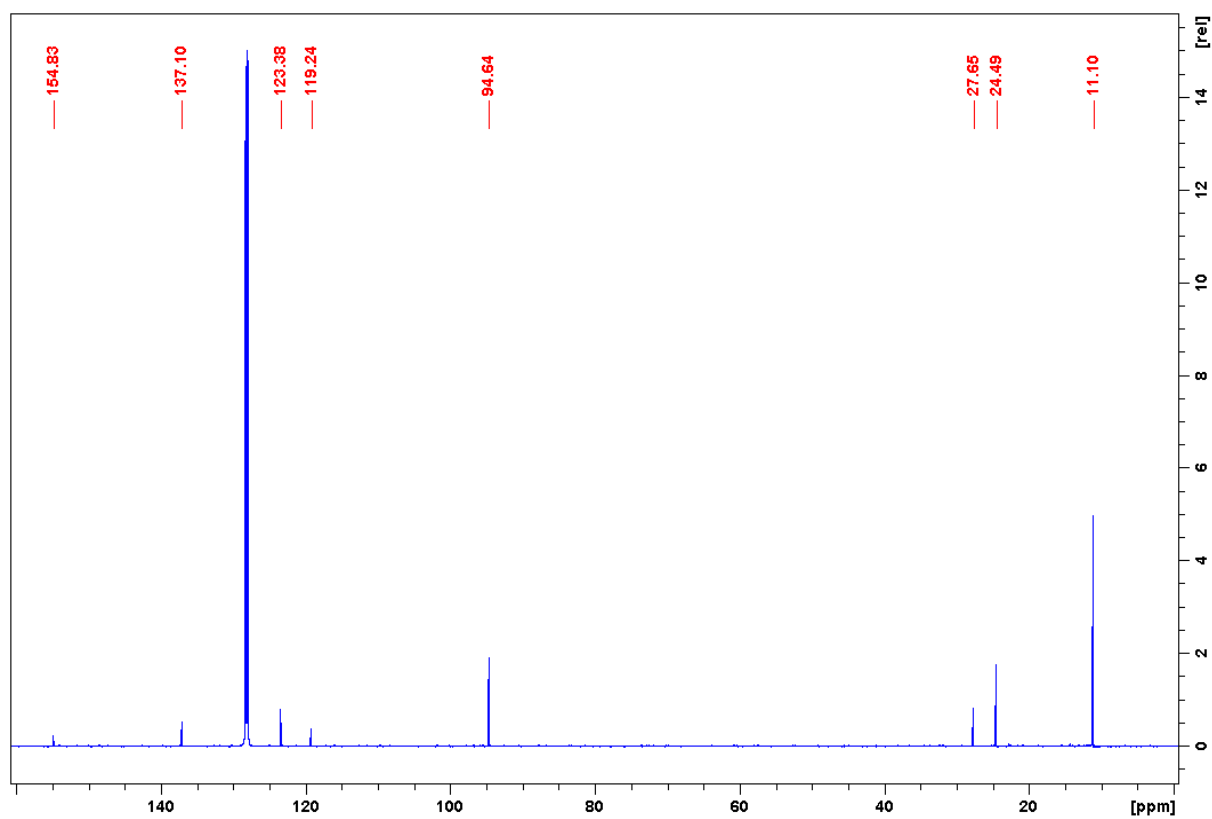


Figure S2. ¹³C{¹H}-NMR spectrum (125 MHz, C₆D₆, 293K) of compound 2-m.

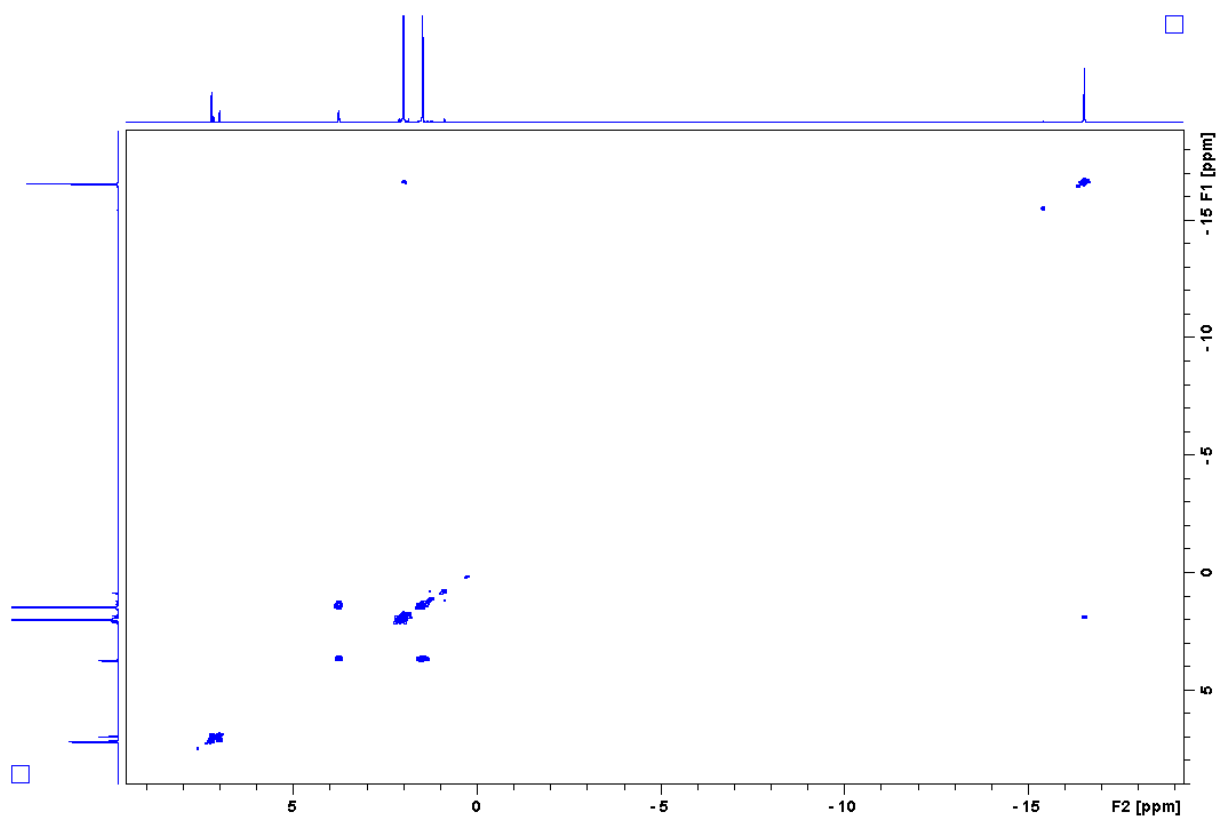


Figure S3. ^1H - ^1H -COSY NMR spectrum (500 MHz, C_6D_6 , 293K) of compound **2-m**.

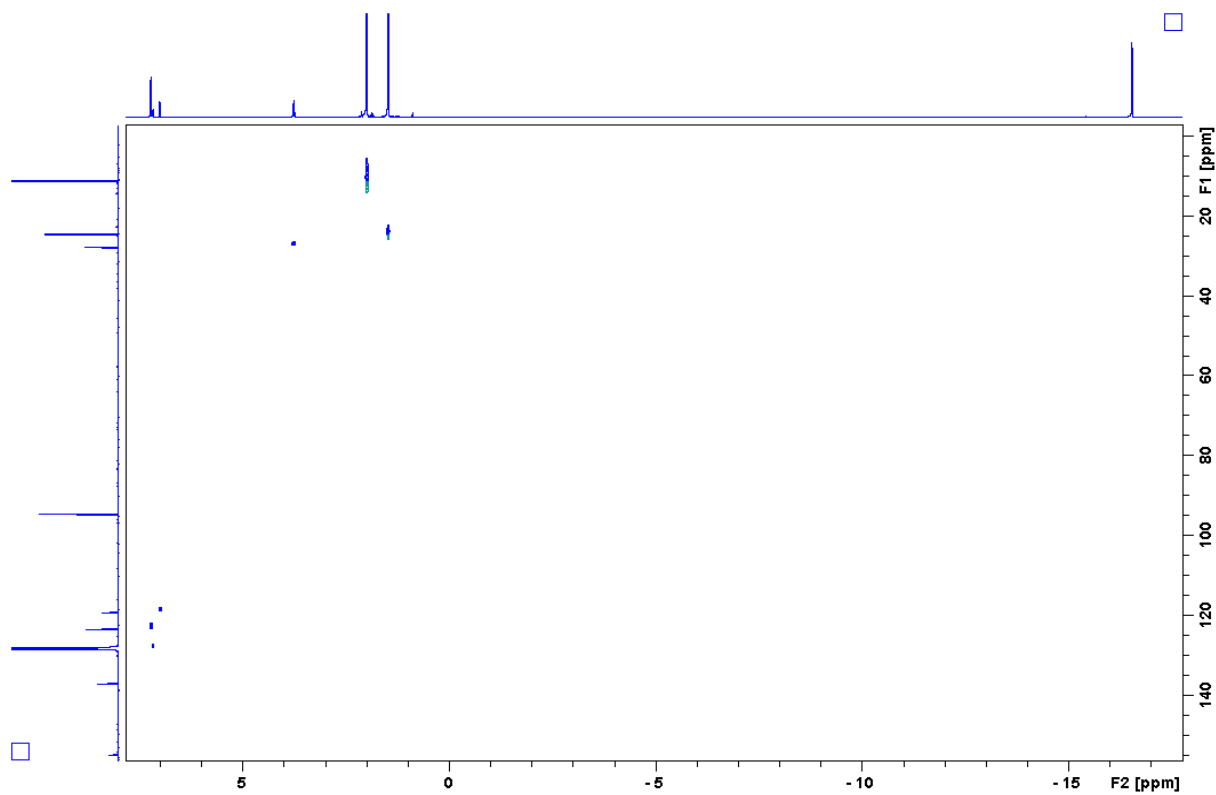


Figure S4. ^1H - ^{13}C -HSQC NMR spectrum (500 MHz, C_6D_6 , 293K) of compound **2-m**.

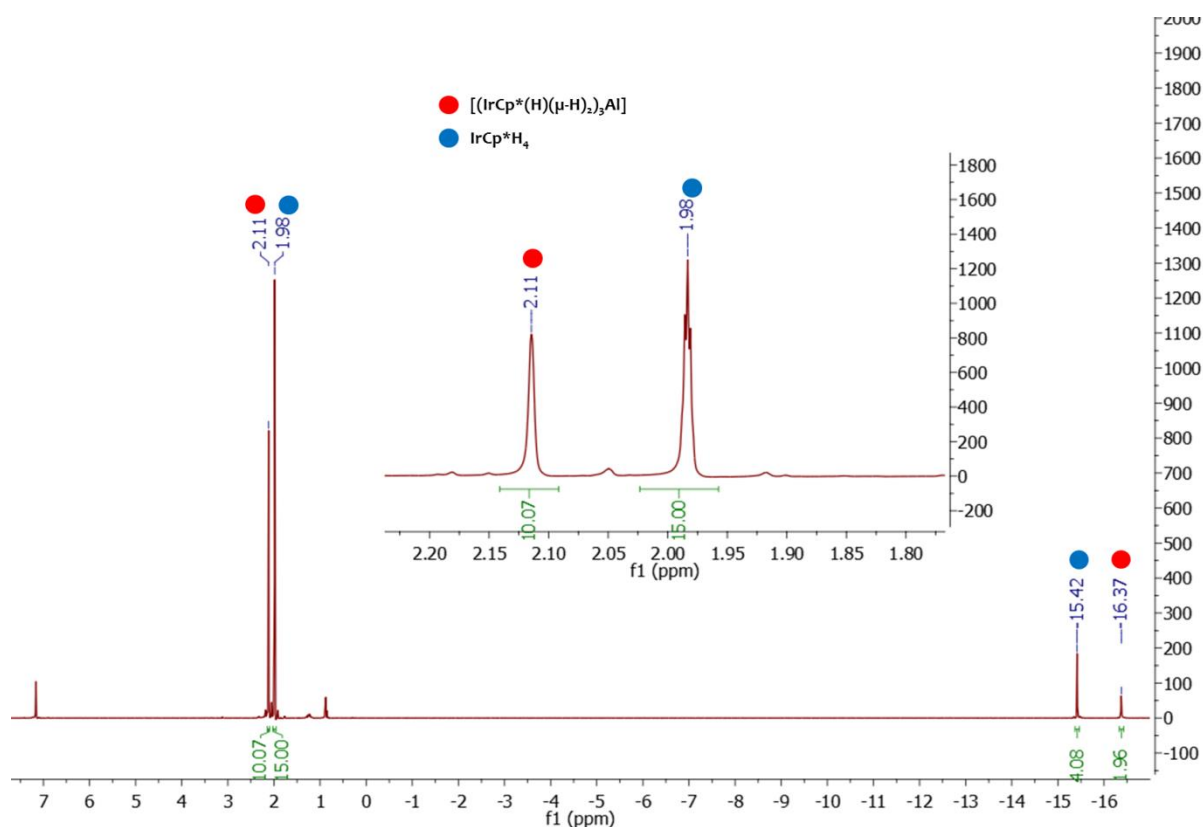


Figure S5. ^1H -NMR spectrum (300 MHz, C_6D_6 , 293K) of the recovered Cp^*IrH_4 and unreacted **1** after reaction of precursor **1** (0.27 mmol, 1.2 eq.) with SBA-15₇₀₀ (0.22 mmol/OH, 1.0 eq.). This reaction leads to the formation of material **2-s** and the reaction coproducts are recovered as white solids (120 mg). Integration of the NMR signals revealed a ratio $\text{Cp}^*\text{IrH}_4/\mathbf{1} = 4.4$, which means the formation of Cp^*IrH_4 (0.22 mmol, 1.0 eq.) along with unreacted **1** (0.05 mmol, 0.2 eq.).

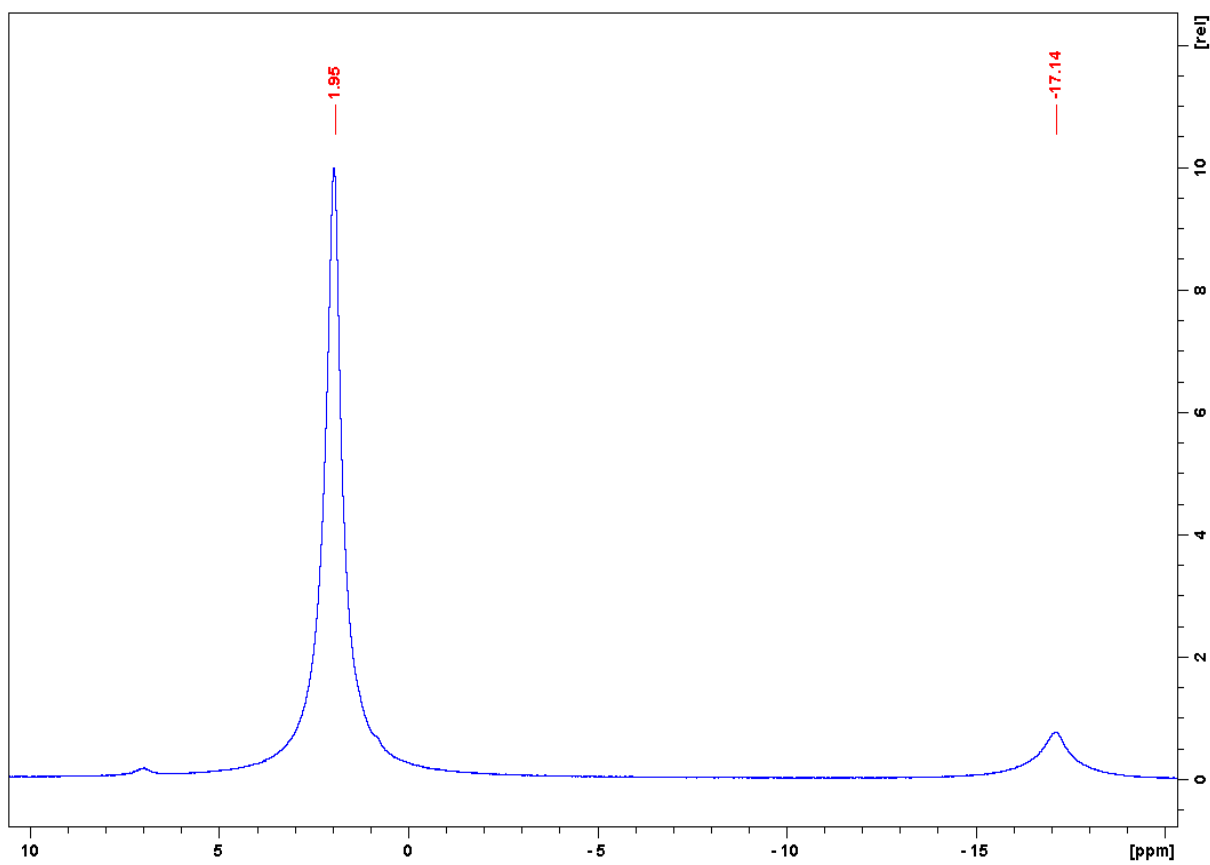


Figure S6. ^1H MAS SSNMR spectrum (293K, 300 MHz, 4 mm probe) of **2-s**.

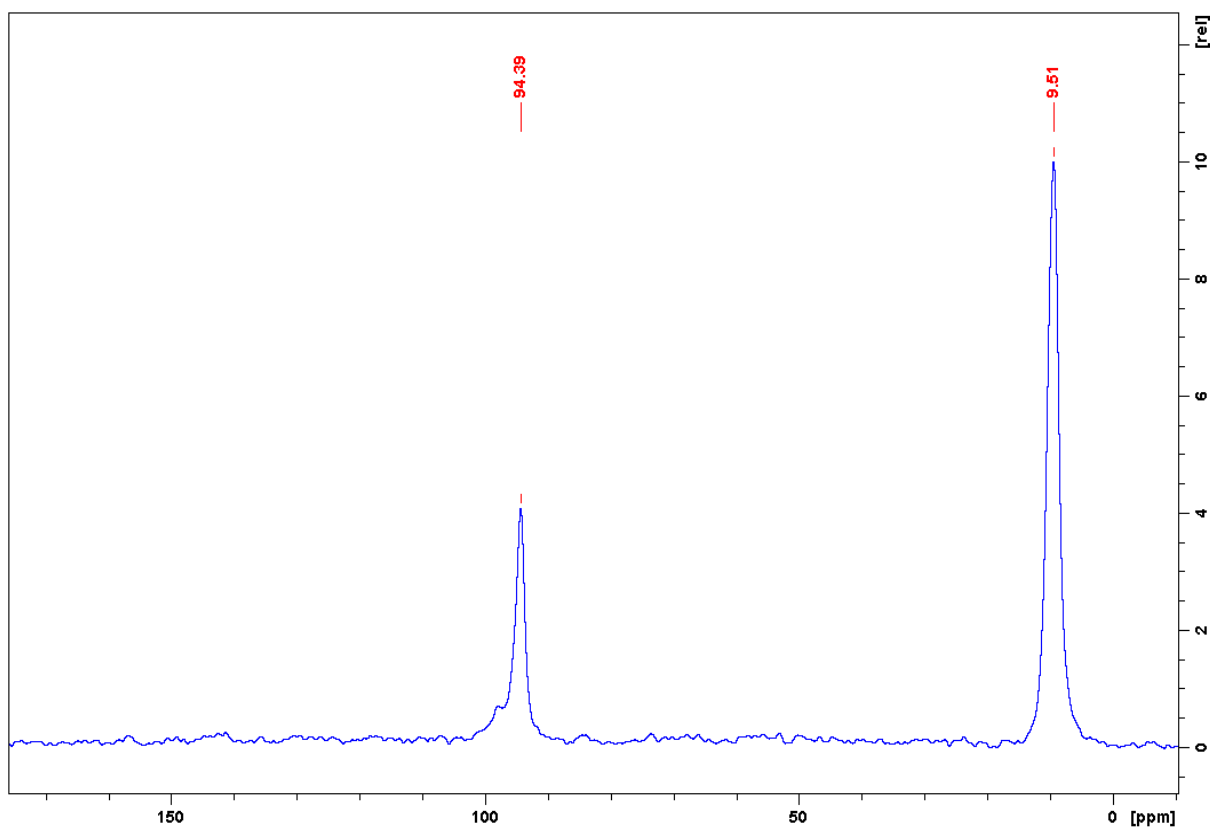


Figure S7. ^{13}C MAS SSNMR spectrum (293K, 75 MHz, 4 mm probe) of **2-s**.

C. IR spectroscopy data

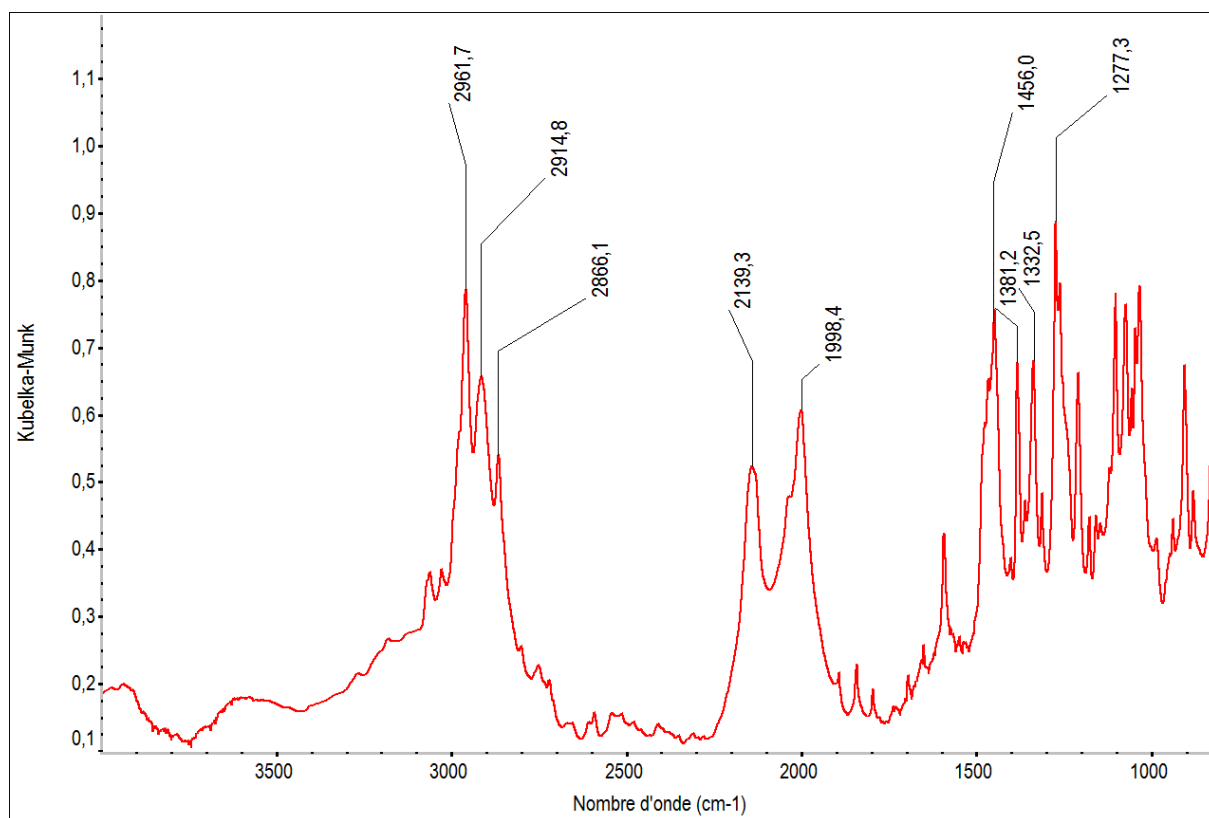


Figure S8. DRIFT spectrum (293K, diluted in KBr, under argon) of compound **2-m**.

D. X-ray crystallography

X-ray structural determinations were performed at the centre de diffractométrie Henri Longchambon, Université de Lyon. A suitable crystal coated in Parabar oil was selected and mounted on a Gemini kappa-geometry diffractometer (Rigaku Oxford Diffraction) equipped with an Atlas CCD detector and using Mo radiation ($\lambda = 0.71073 \text{ \AA}$). Intensities were collected at 150 K by means of the CrysAlisPro software. Reflection indexing, unit-cell parameters refinement, Lorentz-polarization correction, peak integration and background determination were carried out with the CrysAlisPro software. An analytical absorption correction was applied using the modeled faces of the crystal.^[5] The resulting set of hkl was used for structure solution and refinement. The structures were solved by direct methods with SIR97^[6] and the least-square refinement on F^2 was achieved with the CRYSTALS software.^[7] All non-hydrogen atoms were refined anisotropically. The hydrogen atoms were all located in a difference map, but those attached to carbon atoms were repositioned geometrically. The H atoms were initially refined with soft restraints on the bond lengths and angles to regularize their geometry (C---H in the range 0.93--0.98 \AA , O---H = 0.82 \AA) and Uiso(H) (in the range 1.2-1.5 times Ueq of the parent atom), after which the positions were refined with riding constraints. CCDC 2149676 contains the supplementary crystallographic data for this paper. These data are provided free of charge by the Cambridge Crystallographic Data Centre.

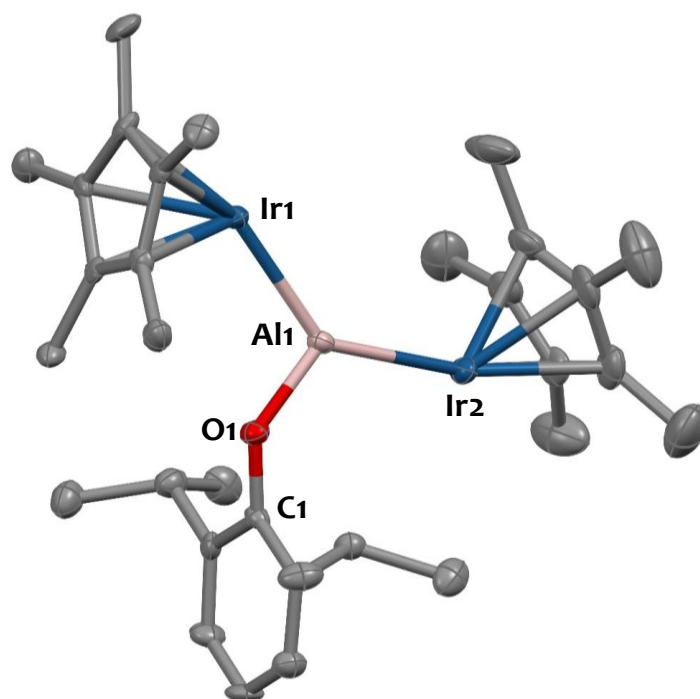


Figure S9. Solid-state molecular structures of **2-m**. Ellipsoids are plotted at a 30% probability level. Hydrogen atoms have been omitted for clarity. Selected bond distances (\AA) and angles ($^\circ$): Ir1-Al1 2.405(4), Ir2-Al1 2.396(4), Al1-O1 1.735(10), O1-C1 1.341(15), Ir2-Al1-Ir1 137.06(17), O1-Al1-Ir1 106.8(4), O1-Al1-Ir2 116.1(4), C1-O1-Al1 135.3(9), Al1-Ir1-Cp*_{centroid} 133.22, Al1-Ir2-Cp*_{centroid} 139.73.

Table S1. Crystallographic parameters for compound **2-m**

Compound	2-m
Formula	C ₃₂ H ₄₇ Allr ₂ O
cryst syst	Monoclinic
space group	P2 ₁ /c
volume (Å ³)	3333.7(3)
a (Å)	8.8760(5)
b (Å)	20.4157(9)
c (Å)	18.4320(9)
α (deg)	90
β (deg)	93.526(4)
γ (deg)	90
Z	4
formula weight (g/mol)	859.07
density (g cm ⁻³)	1.712
absorption coefficient (mm ⁻¹)	8.022
F(000)	1656.0
theta _{max} (°)	29.817
temp (K)	150.00(10)
total no. reflections	44351
independent reflections [R(int)]	8532
no. refined parameters	340
Final R indices [I > 2σ(I)]	R ₁ =0.0767, wR ₂ =0.1824

E. X-ray photoelectron spectroscopy (XPS) data

X-ray photoelectron spectroscopy (XPS) measurements were performed on a Sigma II instrument (Thermo Electron) equipped with an Alpha 110 hemispherical analyzer. The instrument was operated in large area XPS mode using an Al $K\alpha$ X-ray source at 200 W. All samples were prepared in a Ar-glovebox by pressing the sample powder into a piece of indium foil (Alfa Aesar, Puratronic[®] 99.9975% trace metal basis, 0.25 mm thickness). The supported samples were then mounted in a home-made sample holder that allows for the samples to be transferred into the FEAL chamber under vacuum without being exposed to the ambient atmosphere. The pressure in the XPS analysis chamber was maintained under 5.0×10^{-8} mbar during all measurements. Survey scan spectra were collected up to a binding energy of 1100 eV using a pass energy of 50 eV, a step size of 1 eV, and a dwell time of 50 ms. Narrow region scans were collected using a pass energy of 25 eV, a step size of 0.1 eV, and dwell time of 50 ms. All spectra were calibrated to the Si 2p peak of SiO₂ at 103.5 eV. A Shirley background was used when fitting the Ir 4f spectra. The Ir 4f_{7/2} - 4f_{5/2} peak doublet separation was fixed at 2.98 eV and the 4f_{5/2}:4f_{7/2} peak area ratio was fixed at 3:4.

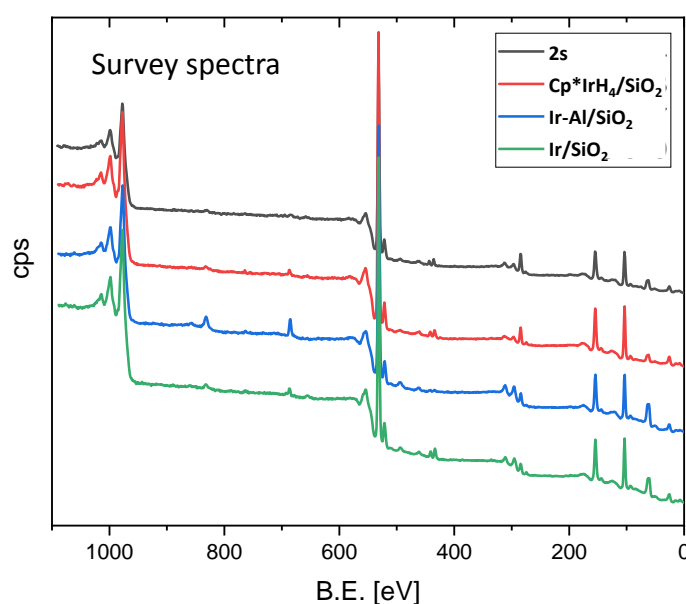


Figure S10. XPS survey spectra for materials **2-s** (black line), **Cp*IrH₄/SiO₂** (red line), **Ir-Al/SiO₂** (blue line) and **Ir/SiO₂** (green line). Some small peaks from the underlying In foil can be seen (In 3d_{5/2} = 444 eV and In 3d_{3/2} = 452 eV). Other In peaks (e.g. 4d@17 eV, 4p@78 eV, 4s@123 eV) are weaker in intensity and are otherwise not expected to overlap with any other regions of interest.

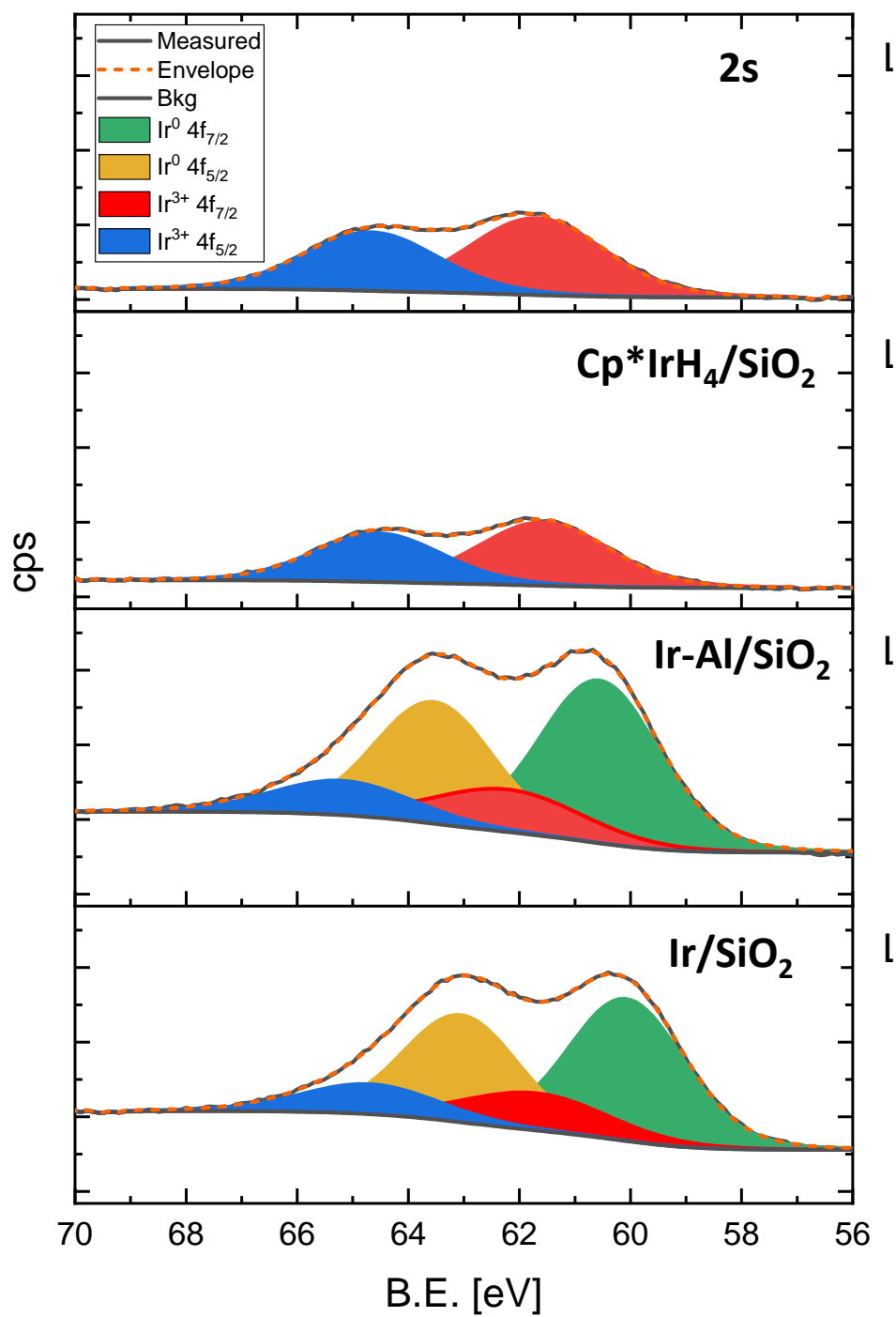


Figure S11. XPS Ir 4f spectra.

Sample	Peak	B.E. [eV]	FWHW [eV]	Area	At.%	Ir(0):Ir(III) ^[a]
2-s	Ir(III) 4f _{7/2}	61.69	2.88	16150	57.1	-
	Ir(III) 4f _{5/2}	64.67	2.83	12132	42.9	
Cp*IrH ₄ /SiO ₂	Ir(III) 4f _{7/2}	61.56	2.76	12773	57.1	-
	Ir(III) 4f _{5/2}	64.54	2.7	9596	42.9	
Al-Ir/SiO ₂	Ir(0) 4f _{7/2}	60.55	2.52	29946	42.93	3.03
	Ir(0) 4f _{5/2}	63.53	2.53	22496	32.25	
	Ir(III) 4f _{7/2}	62.21	3.19	9890	14.18	
	Ir(III) 4f _{5/2}	65.19	2.96	7430	10.65	
Ir/SiO ₂	Ir(0) 4f _{7/2}	60.07	2.46	25441	42.96	3.04
	Ir(0) 4f _{5/2}	63.05	2.44	19112	32.27	
	Ir(III) 4f _{7/2}	61.7	3.08	8374	14.14	
	Ir(III) 4f _{5/2}	64.68	2.88	6291	10.62	

Table S2. XPS Ir 4f data analysis. [a] Ir(0):Ir(III) ratio was calculated as the areas of [Ir(0) 4f_{7/2}+ Ir(0) 4f_{5/2}]/[Ir(III) 4f_{7/2}+ Ir(III) 4f_{5/2}].

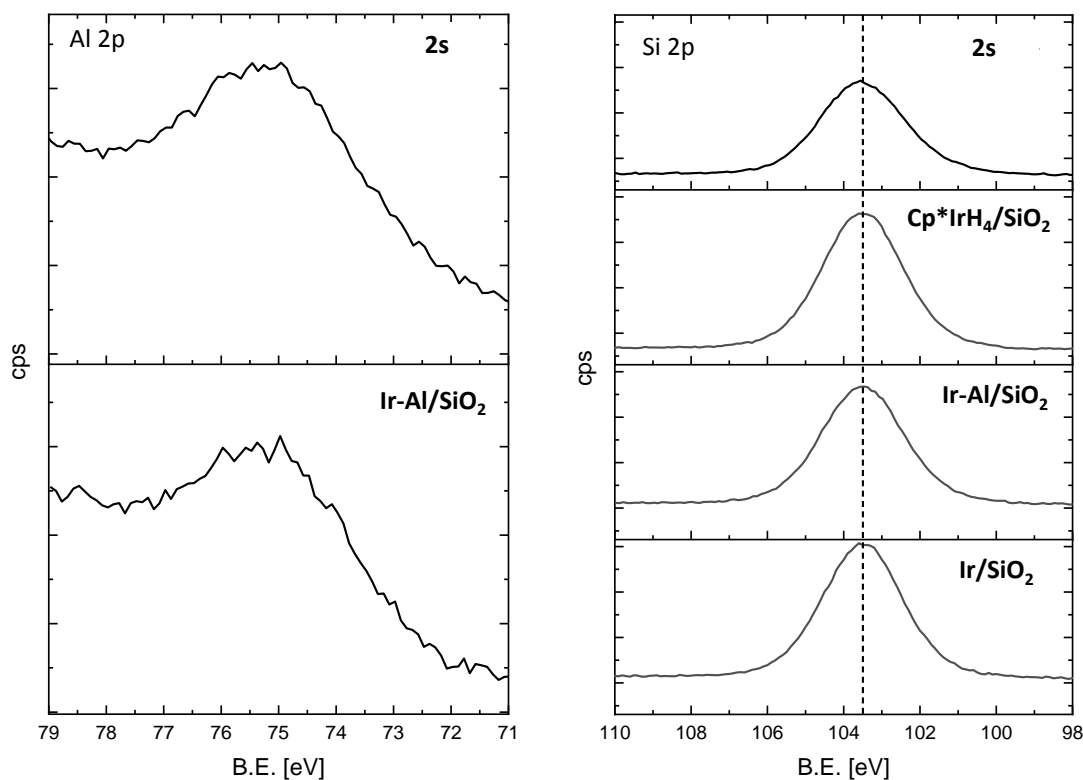


Figure S12. XPS Al 2p and Si 2p data.

F. STEM-HAADF micrographs and EDX data

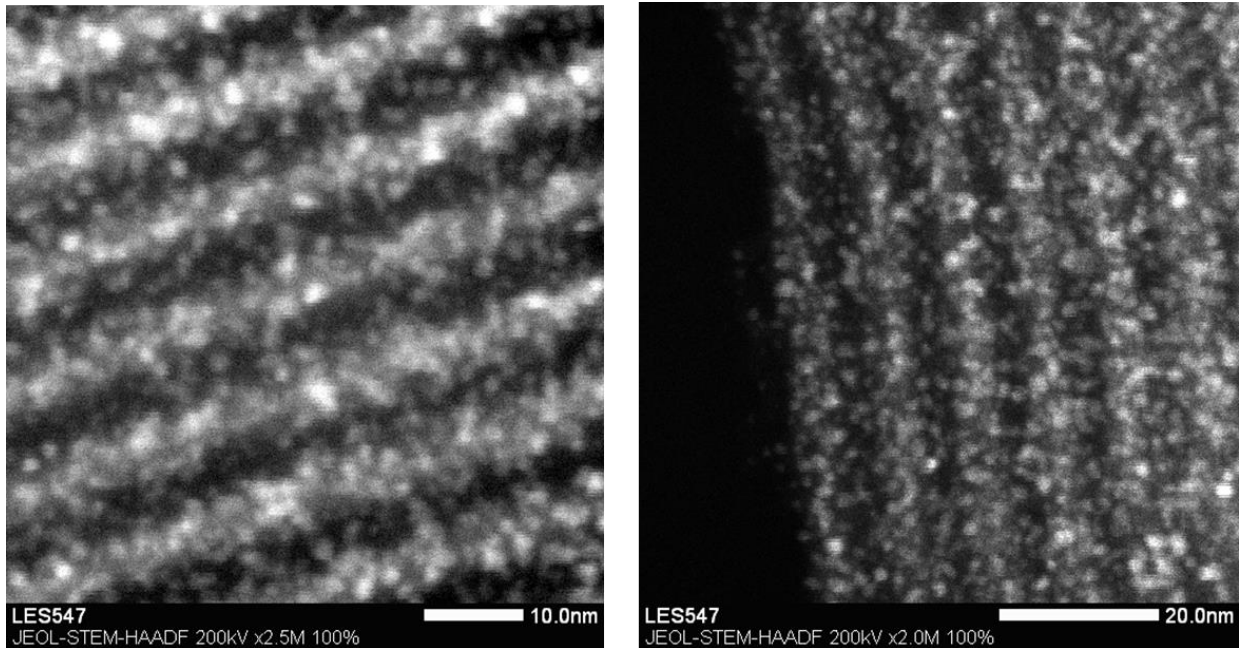


Figure S13. STEM- HAADF micrographs of Ir-Al/SiO₂ showing the formation of metal nanoparticles well dispersed at the surface of the mesostructured channels of the SBA-15₇₀₀ support.

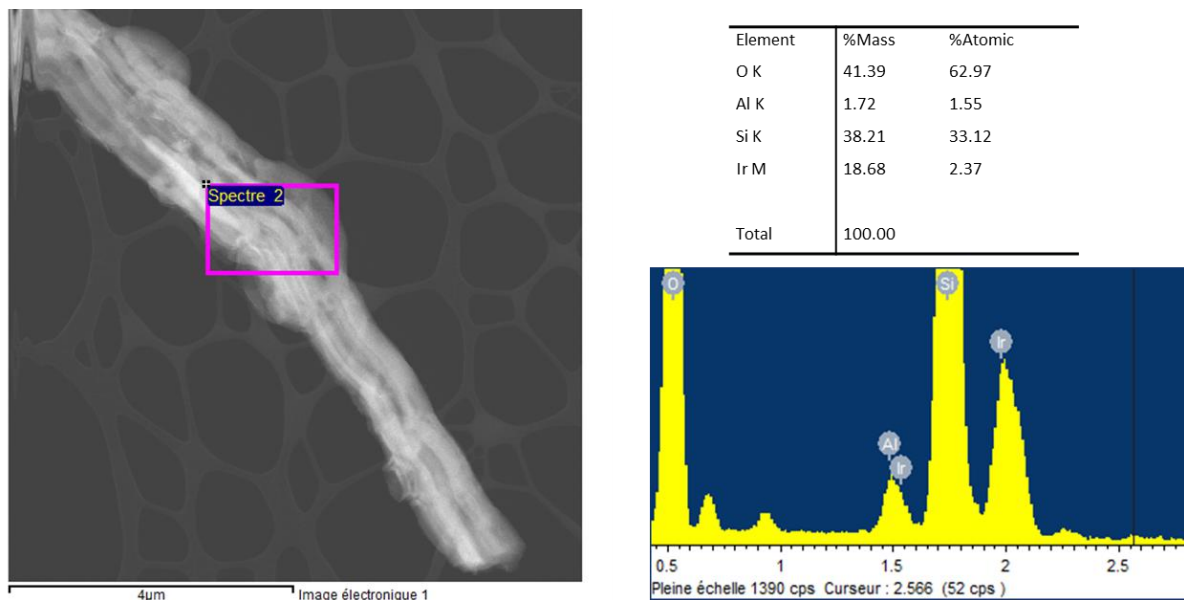


Figure S14. STEM- HAADF micrograph of Ir-Al/SiO₂ (left) and corresponding EDS spectrum (right) recorded on a large zone, showing Al and Ir contributions. Bar scales: 4 μm.

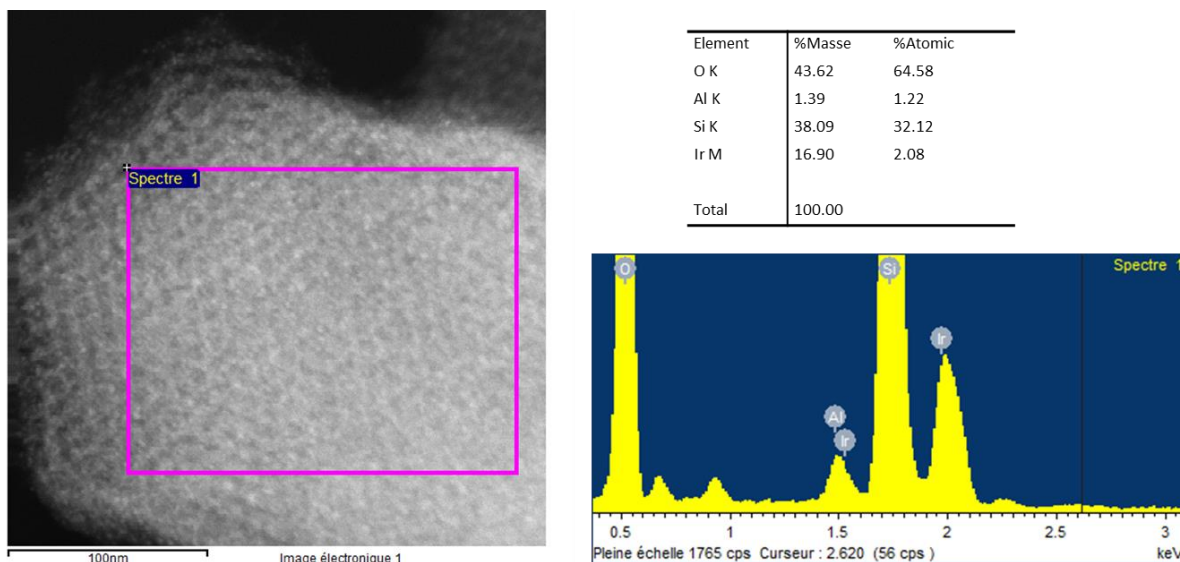


Figure S15. STEM- HAADF micrograph of Ir-Al/SiO₂ (left) and corresponding EDS spectrum (right) recorded on a large zone, showing Al and Ir contributions. Bar scales: 100 nm.

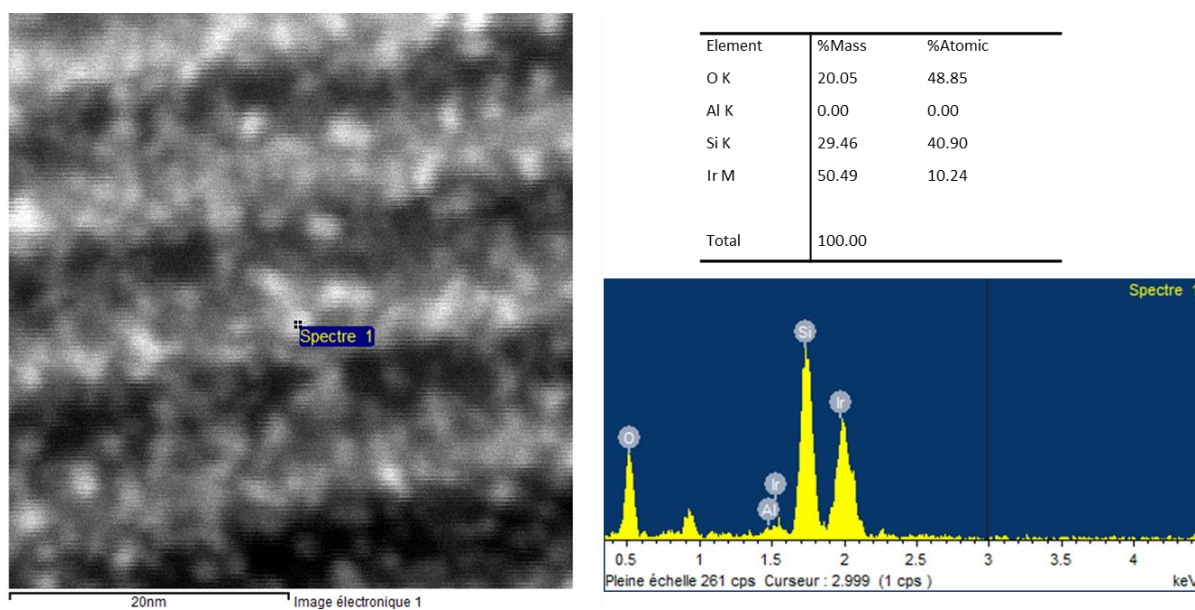


Figure S16. STEM- HAADF micrograph of Ir-Al/SiO₂ (left) and corresponding EDS spectrum recorded on a narrow bright zone (right), in agreement with the formation of a silica-supported Ir NP. Bar scales: 20 nm.

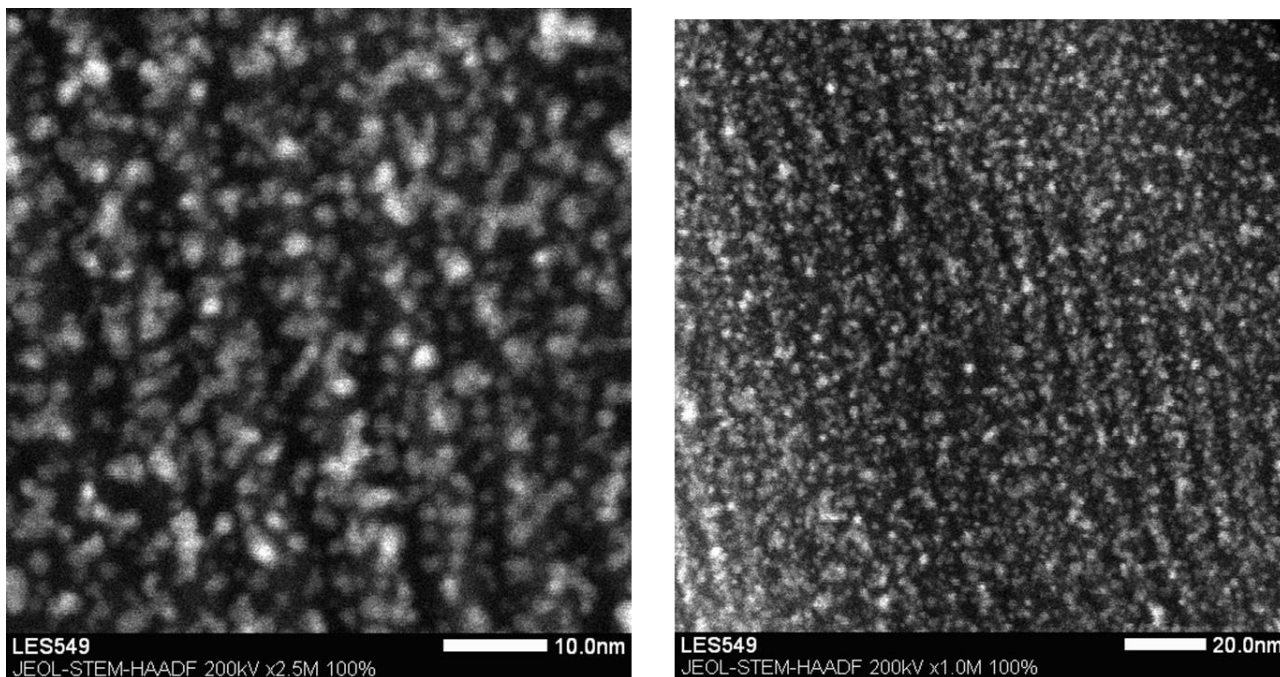


Figure S17. STEM- HAADF micrographs of Ir/SiO_2 showing the formation of metal nanoparticles well dispersed at the surface of the mesostructured channels of the SBA-15₇₀₀ support.

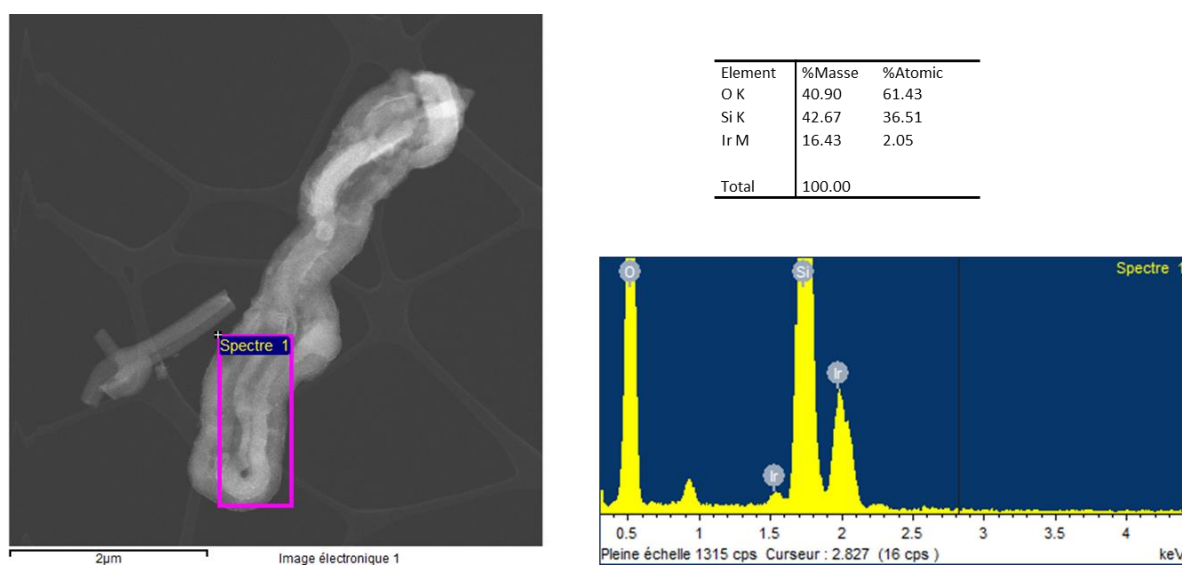


Figure S18. STEM- HAADF micrograph of Ir/SiO_2 (left) and related EDS spectrum (right) recorded on a large zone. Bar scales: 2 µm.

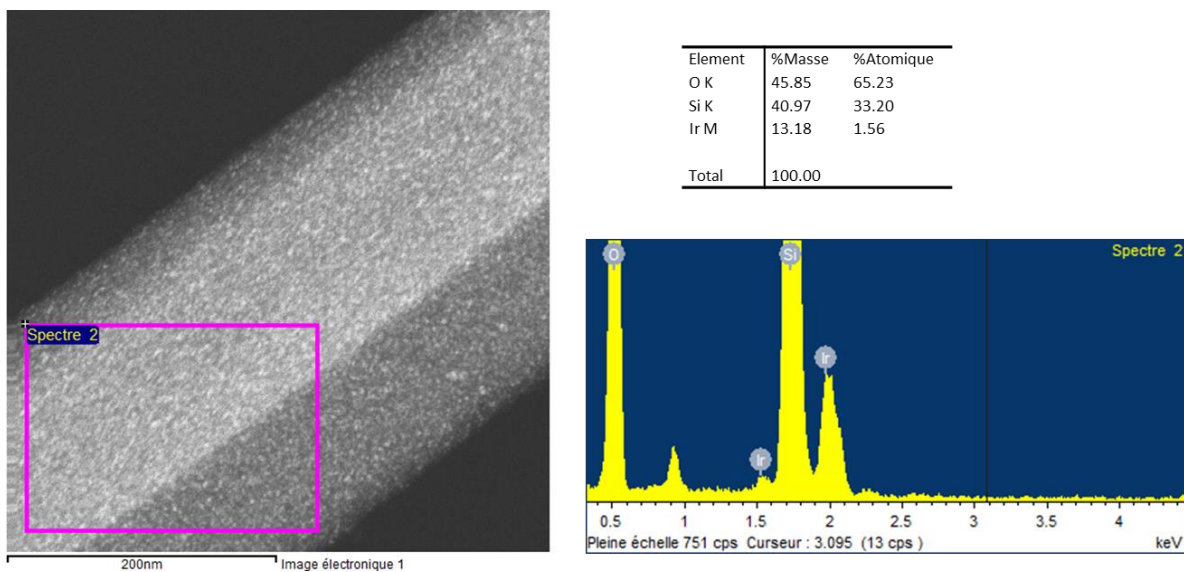


Figure S19. STEM- HAADF micrograph of Ir/SiO₂ (left) and corresponding EDS spectrum (right). Bar scales: 200 nm

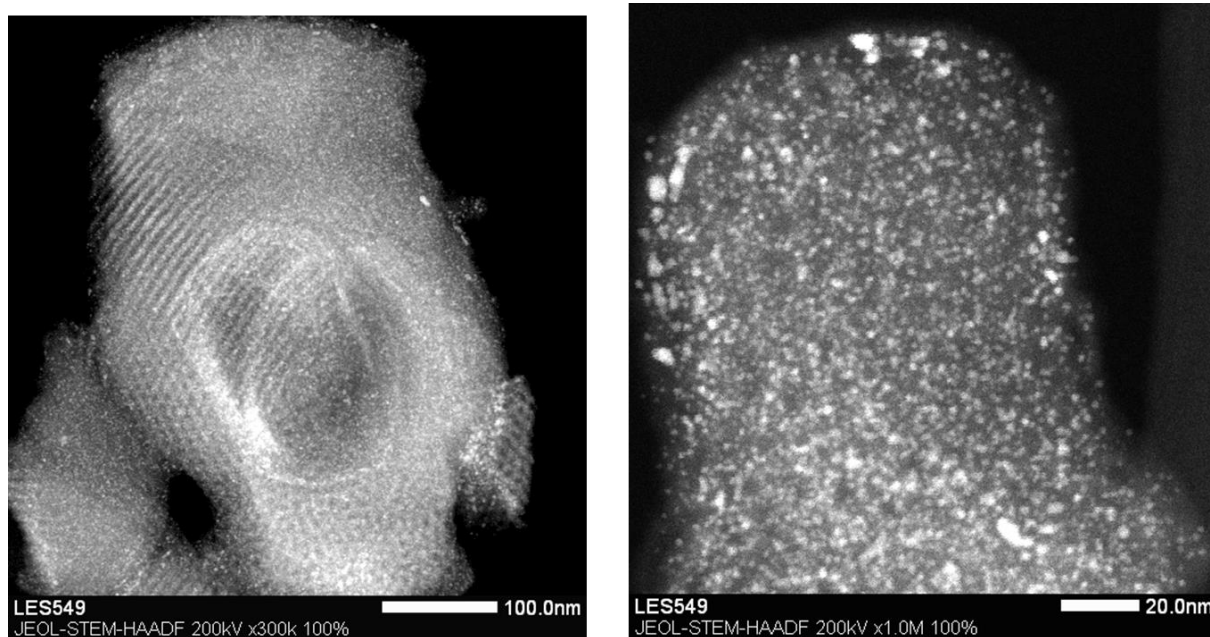


Figure S20. STEM- HAADF micrographs of Ir/SiO₂ showing few Ir larger Nps or aggregates in the range of [3-15 nm].

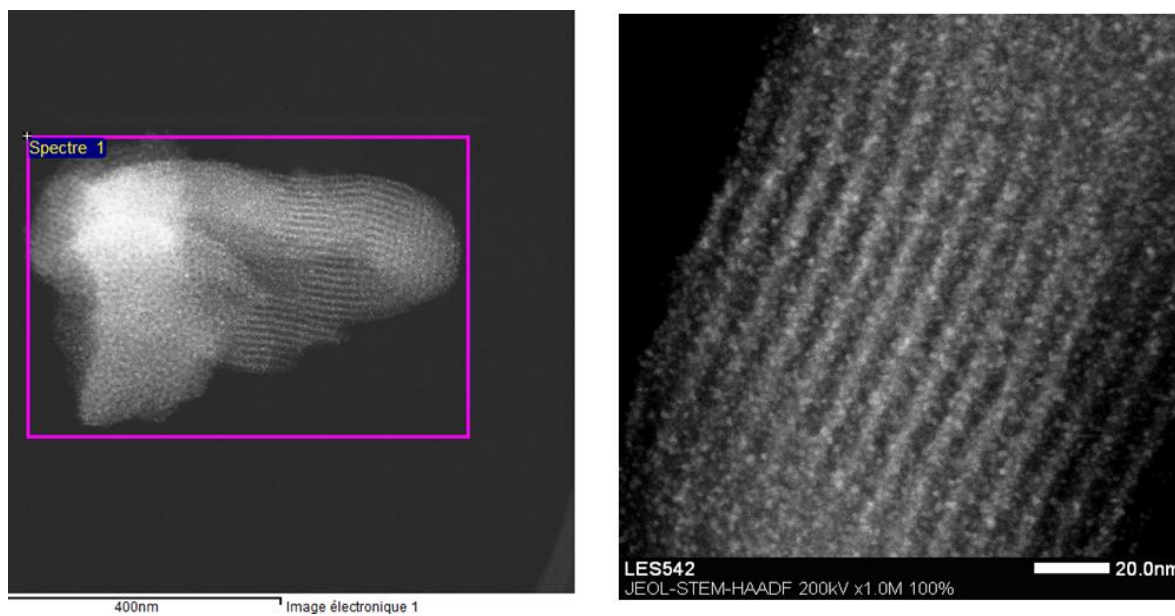


Figure S21. STEM- HAADF micrograph of **Ir-Al/SiO₂** after catalysis showing no noticeable differences compared to **Ir-Al/SiO₂** before catalysis.

G. H₂ Chemisorption studies

G.1 H₂ Chemisorption isotherms

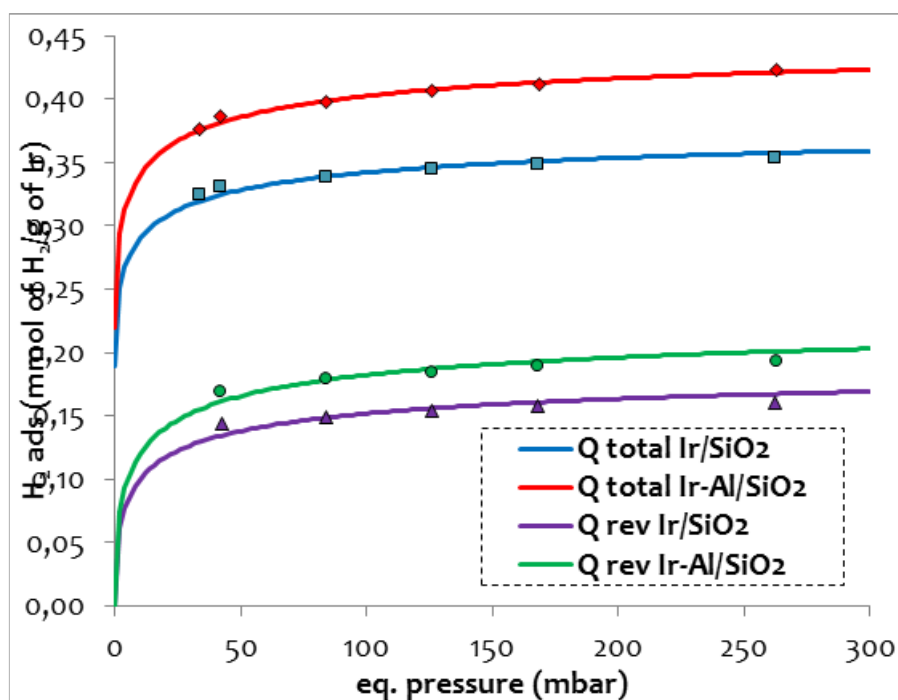


Figure S22. Total H₂ chemisorption isotherms at 298K for Ir NPs from **Ir-Al/SiO₂** - experimental points (red diamonds) and double Langmuir fit (red curve) – and **Ir/SiO₂** - experimental points (blue squares) and double Langmuir fit (blue curve). Reversible H₂ chemisorption isotherm at 298K for Ir NPs from **Ir-Al/SiO₂** - experimental points (green circles) and double Langmuir fit (green curve) – and **Ir/SiO₂** - experimental points (purple triangles) and double Langmuir fit (purple curve).

G.2 Calculation of the dispersion and NPs size

From the double Langmuir fit, we extracted the following parameter: H/Ir_{Total} , which translates the adsorbed atomic hydrogen *per* total iridium atoms. Then, we calculated the dispersion for **Ir-Al/SiO₂** and **Ir/SiO₂** using the equation proposed by F. Drault *et al.*^[8]: $D_{Ir}(\%) = a_{\gamma} (H/Ir)^5 + b_{\gamma} (H/Ir)^4 + c_{\gamma} (H/Ir)^3 + d_{\gamma} (H/Ir)^2 + e_{\gamma} (H/Ir)$ with $a_{\gamma} = -2.116$, $b_{\gamma} = 13.163$, $c_{\gamma} = -20.633$, $d_{\gamma} = -23.073$, and $e_{\gamma} = 100.361$ for iridium. Next, from this dispersion, we calculated the stoichiometric coefficient $H/Ir_{surface}$, which translates to the adsorbed atomic hydrogen *per* surface iridium atoms. Finally, we determined the Ir NPs size using truncated cubic octahedron geometry. Using this strategy, we obtained the following values:

Catalyst	Iridium loading (% wt)	Dispersion (%)	$H/Ir_{surface}$	Avg. NPs size (nm)
Ir-Al/SiO ₂	16.7	67	1.45	1.4
Ir/SiO ₂	18.8	56	1.32	1.7

H. Catalysis

H.1 Procedure

The catalyst powder (ca 10 mg for 1 mol% Ir loadings) was charged in a 480 mL glass reactor and sealed under argon. For low metal loadings of ca 0.1 mol% Ir, the catalyst powder was first diluted in SBA-15₇₀₀ by a factor 10 and the resulting powder was vigorously shaken in a closed 20 mL vial in the glovebox to ensure good mixing. Next, about 10 mg of the resulting light brownish powder was charged in the same reactor. The system was then evacuated on a high-vacuum line (10⁻⁵ mBar) and dry methane (~42 mbars, 0.8 mmol, 1 eq.) and dry deuterium gas (~980 mbars, 19.3 mmol, 24 equiv.) were transferred in the reactor. The reactional medium was heated at 250°C and the gas phase was regularly monitored by GC-MS. The CH_{4-x}D_x (x = 0-4) isotopomers distribution was calculated using the Dibeler and Mohler method as following:^[9]

$$(1) [CD_4] = [m/z=20].$$

$$(2) [CD_3H] = [m/z=19].$$

$$(3) [CD_2H_2] = [m/z=18] - 0.435[CD_3H] - 0.865[CD_4]$$

$$(4) [CDH_3] = [m/z=17] - 0.657[CD_2H_2] - 0.519[CD_3H].$$

$$(5) [CH_4] = [m/z=16] - 0.798[CDH_3] - 0.333[CD_2H_2] - 0.107[CD_3H] - 0.137[CD_4].$$

The isotopomers distribution was also determined using Schoofs approach^[10]:

(0) F1 = [m/z=15]/[m/z=16]; F2 = [m/z=14]/[m/z=16] where F1 and F2 relate respectively to the loss of one and two protons in the CH₄ mass spectrum reference.

$$(1) [CD_4] = [m/z=20]$$

$$(2) [CD_3H] = [m/z=19]$$

$$(3) [CD_2H_2] = [m/z=18] - 0.25F1[CD_3H] - F1[CD_4]$$

$$(4) [CDH_3] = [m/z=17] - 0.5F1[CD_2H_2] - 0.75F1[CD_3H].$$

$$(5) [CH_4] = [m/z=16] - 0.75F1[CDH_3] - 0.5F1[CD_2H_2] - 0.167F2[CD_2H_2] - 0.5F2[CD_3H] - F2[CD_4].$$

The deuteration rate, τ , was determined as followed:

$$\tau_{(t)} = 0.25[CDCH_3]_t + 0.5[CD_2H_2]_t + 0.75 [CD_3H]_t + [CD_4]_t$$

From these data, the following kinetic graphs can be plotted: percentage of each CH_{4-x}D_x isotopomers = f(t), distribution of deuteromethanes = f(methane conversion), τ = f(t), TON = f(t), and TON_{surface} = f(t). The TON = f(t) curves were fitted by polynomial equations of degrees 3, 4, 5 or 6 in view of accurately calculating the different kinetic parameters (TOF especially). For the catalysis, an induction time of 5 minutes was noticed that corresponds to the thermic transfer into the reactor, *i.e.* the time to reach the desired temperature in the system. Therefore, time origin of the graphs corresponds to this induction time, the maximum turnover frequency (TOF_{max}) was also calculated after this period of 5 minutes.

H.2 Kinetic graphs

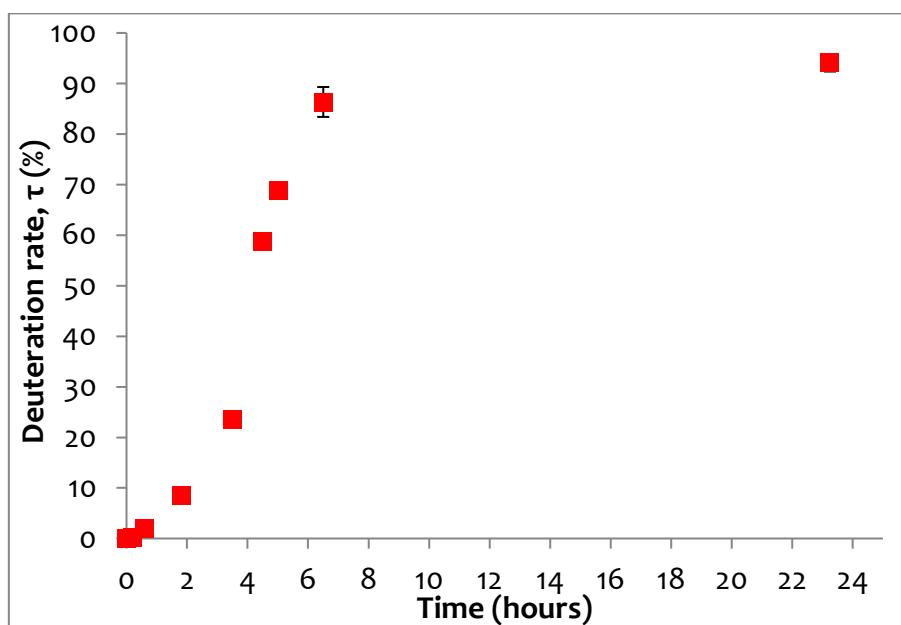


Figure S23. CH_4 deuteration rate as a function of reaction time at $T=250^\circ\text{C}$ for precatalyst **2-s** (red squares) at 1.0 mol%/Ir. This graph shows a long induction time of about 4 hours. This is attributed to the in-situ formation of metal Nps, which are active in catalysis. All the data were extracted by averaging Dibeler-Mohler and Schoofs calculations. Errors bars relate to the standard deviation between Dibeler-Mohler and Schoofs calculations.

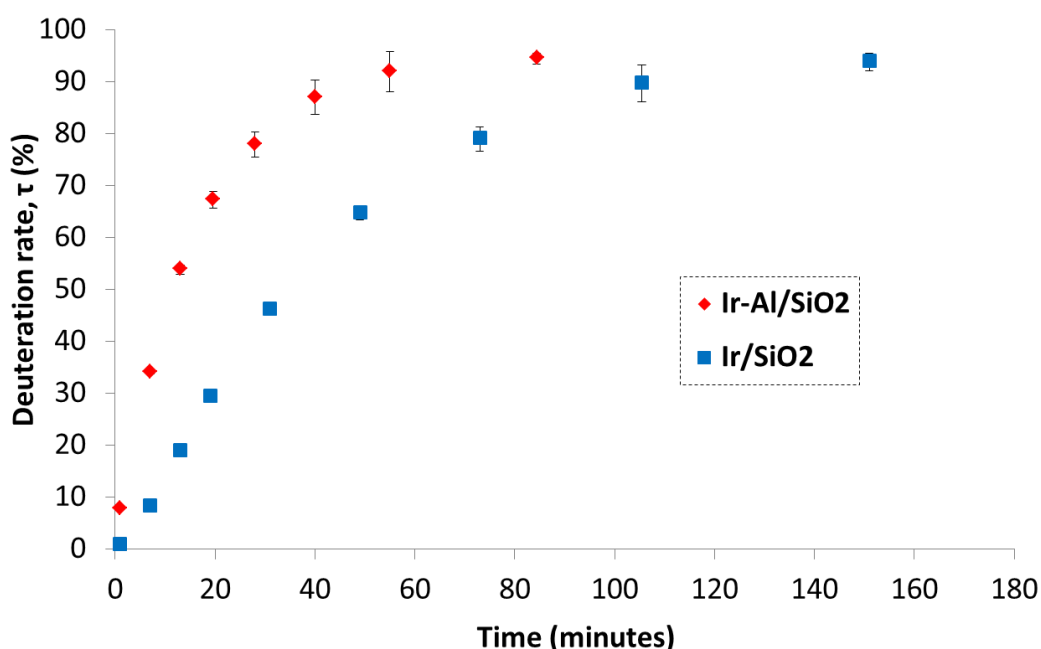


Figure S24. CH_4 deuteration rate as a function of reaction time at $T=250^\circ\text{C}$ for catalyst **Ir-Al/SiO₂** (red diamonds) at 1.0 mol%/Ir; and **Ir/SiO₂** (blue squares) at 1.2 mol%/Ir *i.e.* 0.67 mol% Ir surface sites for both catalysts. All the data were extracted by averaging Dibeler-Mohler and Schoofs calculations. Errors bars account on the standard deviation between Dibeler-Mohler and Schoofs calculations.

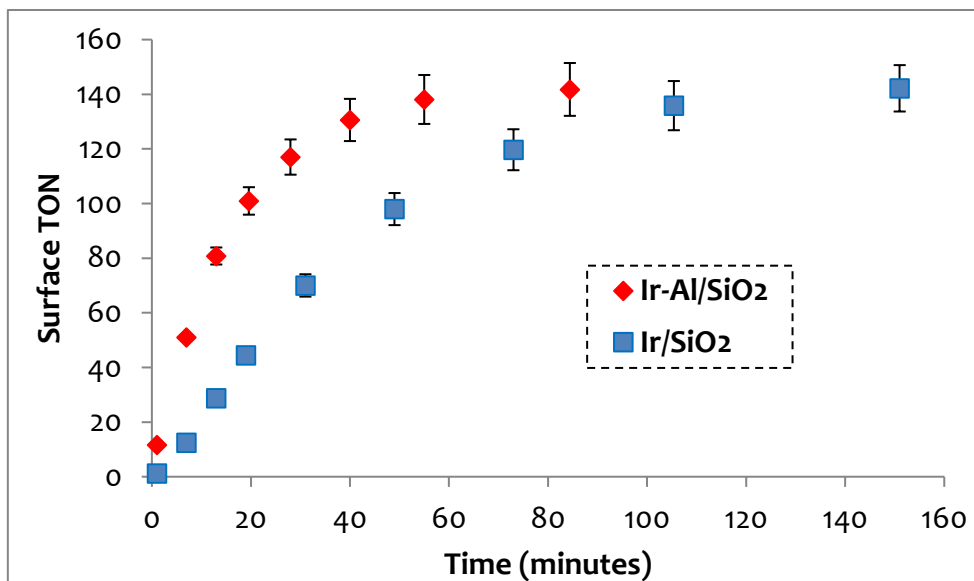


Figure S25. Surface turnover number (TON for surface iridium) as a function of reaction time at $T=250^{\circ}\text{C}$ for catalyst **Ir-Al/SiO₂** (red diamonds) at 1.0 mol%/Ir; and **Ir/SiO₂** (blue squares) at 1.2 mol%/Ir *i.e.* 0.67 mol% Ir surface sites for both catalysts. All the data were extracted by averaging Dibeler-Mohler and Schoofs calculations. Errors bars account for uncertainties on the weighing scale (± 0.5 mg) and also on the standard deviation between Dibeler-Mohler and Schoofs calculations.

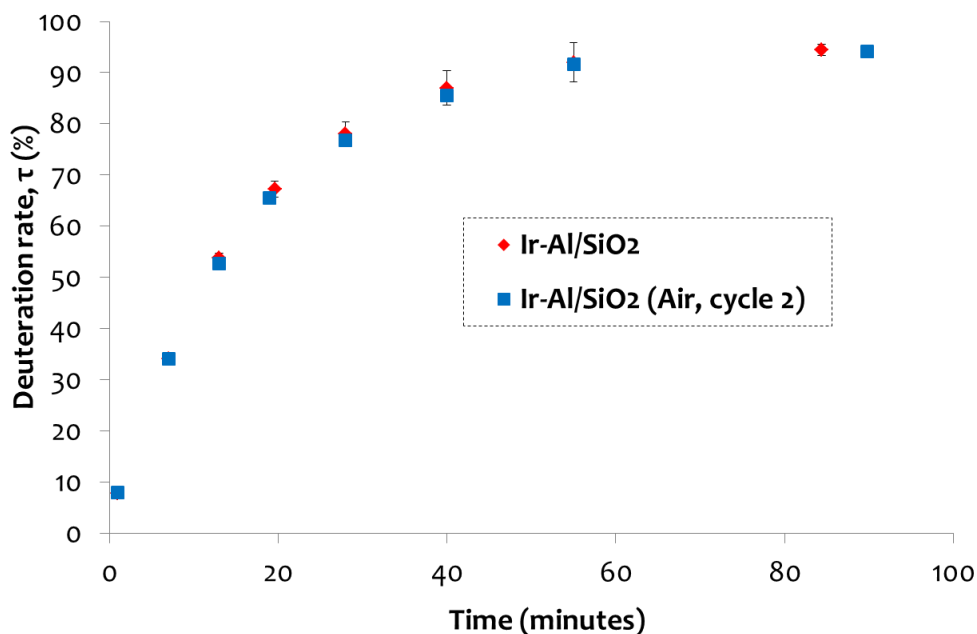


Figure S26. CH₄ deuteration rate as a function of reaction time at $T=250^{\circ}\text{C}$ for catalyst **Ir-Al/SiO₂** at 1.0 mol%/Ir. A first catalytic cycle (red diamonds) is performed, then the reactor is exposed to air for 1 hour before running a second catalytic cycle (blue squares). All the data were extracted by averaging Dibeler-Mohler and Schoofs calculations. Errors bars relate to the standard deviation between Dibeler-Mohler and Schoofs calculations.

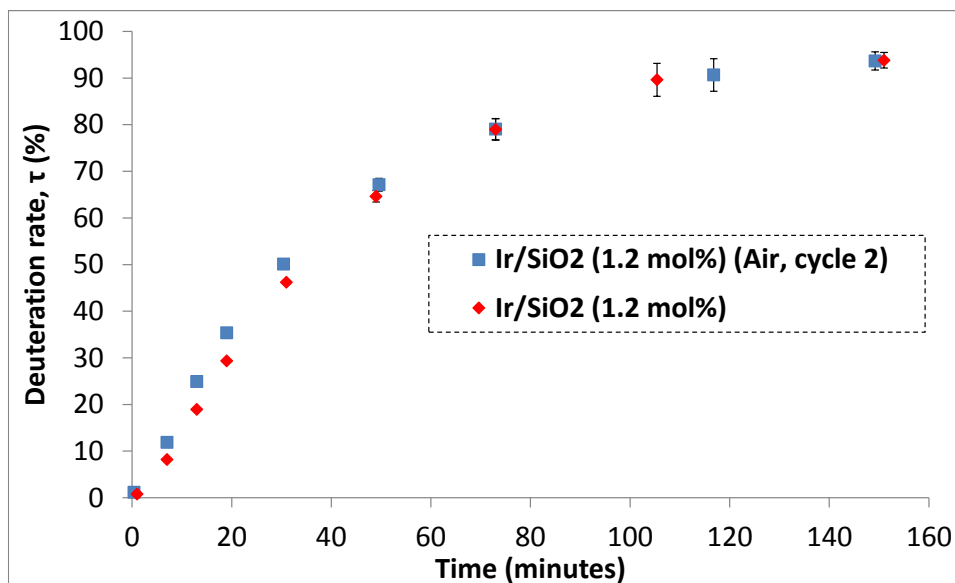


Figure S27. CH₄ deuteration rate as a function of reaction time at T=250°C for catalyst Ir/SiO₂ at 1.2 mol%/Ir. A first catalytic cycle (red diamonds) is performed, then the reactor is exposed to air for 1 hour before running a second catalytic cycle (blue squares). All the data were extracted by averaging Dibeler-Mohler and Schoofs calculations. Errors bars relate to the standard deviation between Dibeler-Mohler and Schoofs calculations.

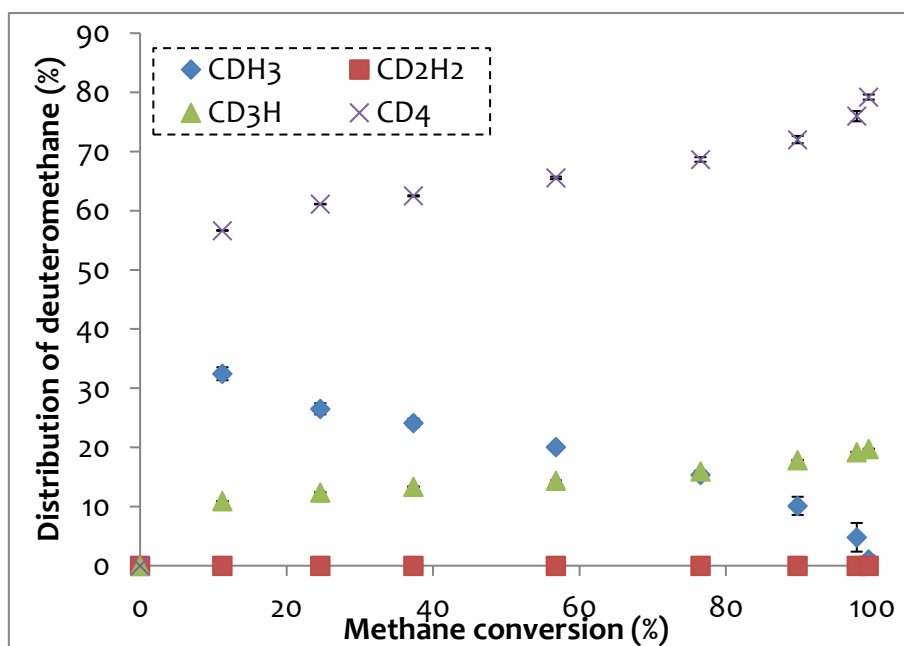


Figure S28. Distribution of deuteromethanes as a function of methane conversion for Ir/SiO₂. All the data were extracted by averaging Dibeler-Mohler and Schoofs calculations. Errors bars relate to the standard deviation between Dibeler-Mohler and Schoofs calculations.

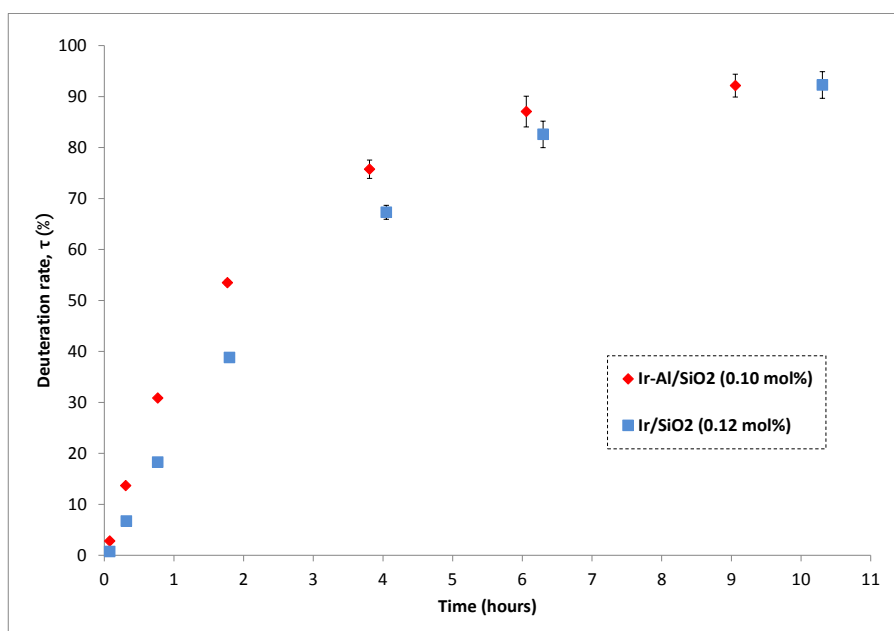


Figure S29. CH₄ deuteration rate as a function of reaction time at T=250°C for catalyst Ir-Al/SiO₂ (red diamonds) at 0.10 mol%/Ir; and Ir/SiO₂ (blue squares) at 0.12 mol%/Ir *i.e.* 0.067 mol% Ir surface sites for both catalysts. All the data were extracted by averaging Dibeler-Mohler and Schoofs calculations. Errors bars account on the standard deviation between Dibeler-Mohler and Schoofs calculations.

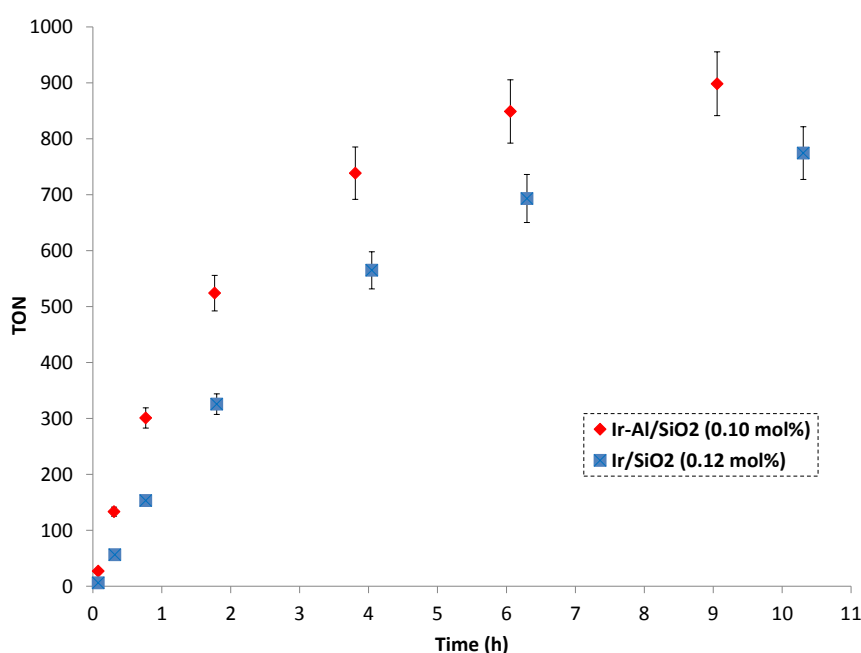


Figure S30. Turnover number (TON) as a function of reaction time at T=250°C for catalyst Ir-Al/SiO₂ (red diamonds); and Ir/SiO₂ (blue squares) at 0.10 mol% and 0.12 mol% respectively, *i.e.* 0.067 mol% Ir surface sites. All the data were extracted by averaging Dibeler-Mohler and Schoofs calculations. Errors bars account for uncertainties on the catalyst loading and on the standard deviation between Dibeler-Mohler and Schoofs calculations. The catalysts turnover numbers are calculated as follow: $TON = \tau \cdot n_{CH_4} / n_{Ir}$ where n_{Ir} is the total number of moles of iridium in the catalyst.

H.3 Mechanistic considerations

First of all, it is worth mentioning that the exchange of H and D on metal catalysts is known to be much faster than the activation of the C-H/D bonds,^[11,12] thus the mobile hydrides on the surface are rapidly exchanged with deuterides in presence of excess D₂ and it is assumed that these events are not rate determining. Two main mechanisms are known for methane H/D exchange on noble metal surfaces: (i) stepwise exchange (Figure S29) and (ii) multiple exchange (Figure S30).^[11,13,14] The first step in both mechanisms is the chemisorption of CH_{4(g)} which cleaves a C-H bond and gives alkyl and hydride fragments *via* a process analogous to an oxidative addition. In the stepwise exchange mechanism (Figure S29), the C-H activations of the surface methyl fragment subsequent to adsorption are slower than the desorption step, therefore monodeuteromethane (CDH₃) is the major product at low conversion with negligible amount of CD₄. In contrast, in a multiple exchange mechanism (Figure S30) the rate determining step is the adsorption/desorption of CH₄ and the C-H activations subsequent to adsorption are fast. It is possible that these subsequent C-H activations result from the rapid dissociation and recombination of the adsorbed methyl groups to form methylidene groups.^[11,13,14] This gives CD₄ (full deuteration) as major product at low CH₄ conversion. The distribution of each isotopomers as a function of conversion is therefore an excellent way to obtain mechanistic insights, as was reported before with various metal catalysts.^[11,13,14] Of course these are two extreme mechanisms: both mechanisms can occur concomitantly to some extent and the distribution of products depends on the relative rates of each steps.

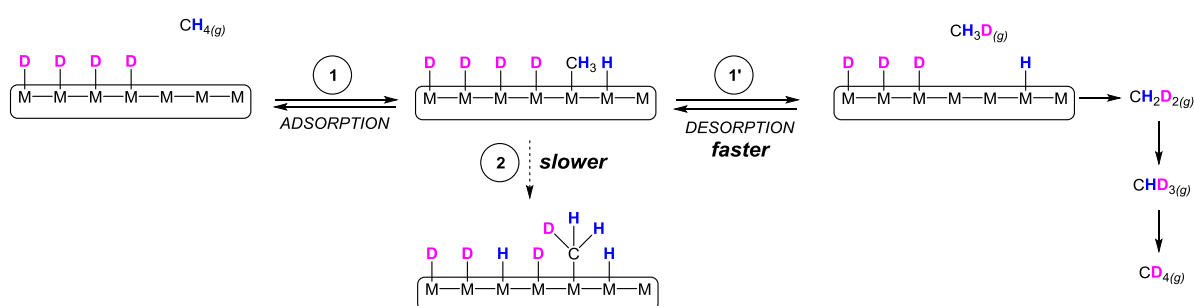


Figure S31. Mechanism for stepwise exchange between CH₄ and excess D₂ on a noble metal catalyst, which is expected to give CH₃D as major product at low conversion.

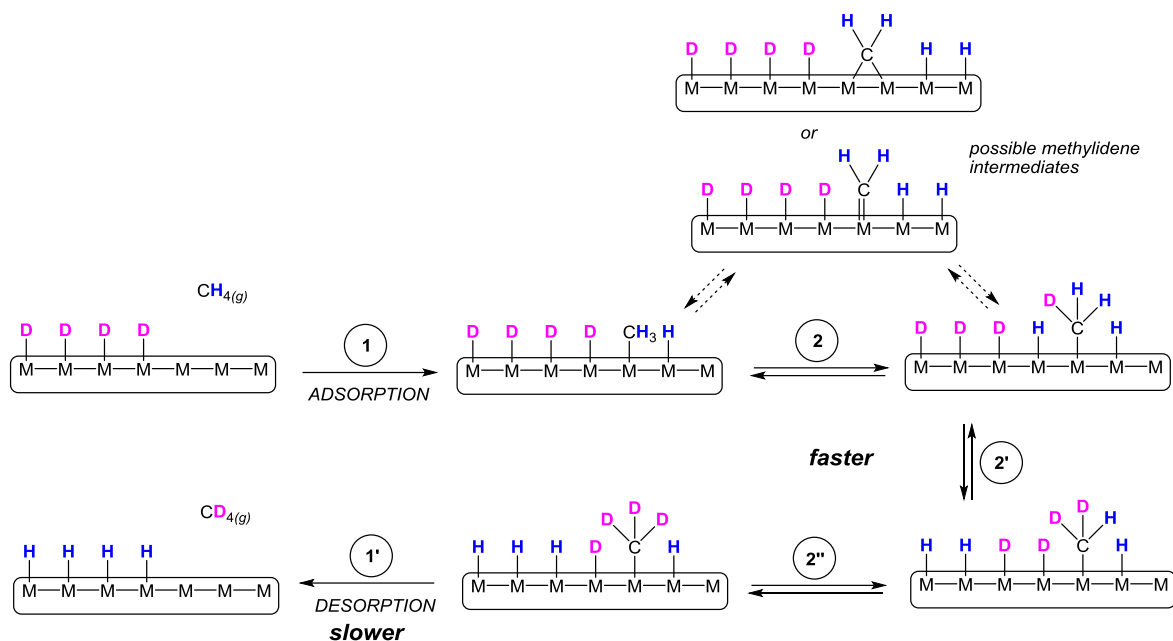


Figure S32. Mechanism for multiple exchange between CH_4 and excess D_2 on a noble metal catalyst, which is expected to give CD_4 as major product at low conversion.

In the present case, the distribution of isotopomers as a function of methane conversion are roughly similar for both catalysts, Ir/SiO_2 and $\text{Ir-Al}/\text{SiO}_2$. CD_4 is the major isotopomer (>55%) at low conversion (<15%) which suggests an important contribution of a multiple exchange mechanism in both cases on the Ir Nps. In such mechanism, the rate determining step is the CH_4 dissociative adsorption step, which may be facilitated by the presence of the Al^{3+} sites at the direct proximity of the Ir particles.

Note that H/D exchange of CH_4 can be promoted by metal oxides, such as dehydrated γ -alumina, through a mechanism in which CH_4 is dissociatively adsorbed across the Al-O moieties (Figure S31-top).^[15,16] Alternatively, molecular early metal hydrides (eg. Zr) can activate methane through a σ -bond metathesis mechanism (Figure S31-bottom).^[17,18] In these two mechanisms, stepwise exchange producing CH_3D at low conversion is the only reported exchange distribution shown in the literature thus far.^[11] These mechanisms are thus unlikely in the present case.

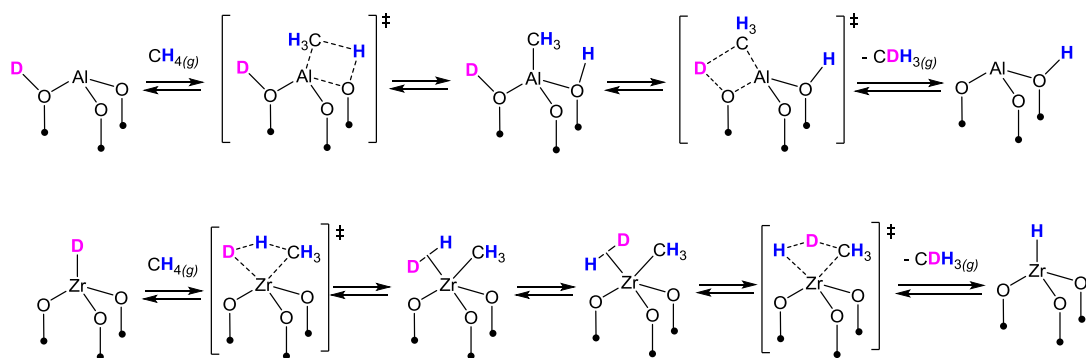


Figure S33. Metal-ligand (top) and sigma bond metathesis (bottom) mechanisms for exchange between CH_4 and excess D_2 , which both give CH_3D as major product at low conversion.

I. Authors contributions and acknowledgements

L.E. performed the syntheses and the catalytic tests. L.V. did the TEM and chemisorption studies. D.F.A. and V.M. performed the XPS studies. L.E., D.F.A., V.M., L. V., C.T. and C.C. curated the data. L.E., D.F.A., V.M., L.V., C.T. and C.C. participated to the writing and revising of the draft. C.T. and C.C. supervised the work. C.C. found the funds and administrated the project. This research was performed in the frame of a project funded by the French National Research Agency (ANR) (grant number ANR-21-CE07-0009-01 (SHICC)). We thank Nesrine Oueslati for her help with the solid-state NMR measurements and Erwann Jeanneau from the “Centre de diffractométrie Henri Longchambon, Université Claude Bernard Lyon-1”, for the XRD analysis. There are no conflicts to declare.

J. References

- [1] L. Escomel, N. Soulé, E. Robin, I. Del Rosal, L. Maron, E. Jeanneau, C. Thieuleux, C. Camp, *Inorg. Chem.* **2022**, acs.inorgchem.1c03120.
- [2] T. M. Gilbert, F. J. Hollander, R. G. Bergman, *J. Am. Chem. Soc.* **1985**, *107*, 3508–3516.
- [3] R. J. P. Corriu, Y. Guari, A. Mehdi, C. Reyé, C. Thieuleux, L. Datas, *Chem. Commun.* **2001**, *37*, 763–764.
- [4] C. Copéret, A. Comas-Vives, M. P. Conley, D. P. Estes, A. Fedorov, V. Mougél, H. Nagae, F. Núñez-Zarur, P. A. Zhizhko, *Chem. Rev.* **2016**, *116*, 323–421.
- [5] R. C. Clark, J. S. Reid, *Acta Crystallogr. Sect. A Found. Crystallogr.* **1995**, *51*, 887–897.
- [6] A. Altomare, M. C. Burla, M. Camalli, G. L. Casciarano, C. Giacovazzo, A. Guagliardi, A. G. G. Moliterni, G. Polidori, R. Spagna, *J. Appl. Crystallogr.* **1999**, *32*, 115–119.
- [7] P. W. Betteridge, J. R. Carruthers, R. I. Cooper, K. Prout, D. J. Watkin, *J. Appl. Crystallogr.* **2003**, *36*, 1487–1487.
- [8] F. Drault, C. Comminges, F. Can, L. Pirault-Roy, F. Epron, A. Le Valant, *Materials (Basel)*. **2018**, *11*, DOI 10.3390/ma11050819.
- [9] F. L. Mohler, V. H. Dibeler, E. Quinn, *J. Res. Natl. Bur. Stand. (1934)*. **1958**, *61*, 171.
- [10] B. Schoofs, J. A. Martens, P. A. Jacobs, R. A. Schoonheydt, *J. Catal.* **1999**, *183*, 355–367.
- [11] A. Sattler, *ACS Catal.* **2018**, *8*, 2296–2312.
- [12] R. L. Burwell, *Acc. Chem. Res.* **1969**, *2*, 289–296.
- [13] C. Kemball, *Proc. R. Soc. London. Ser. A. Math. Phys. Sci.* **1953**, *217*, 376–389.
- [14] A. Frennet, <http://dx.doi.org/10.1080/01614947408079626> **2006**, *10*, 37–68.
- [15] R. Wischert, C. Copéret, F. Delbecq, P. Sautet, *Angew. Chemie Int. Ed.* **2011**, *50*, 3202–3205.

- [16] J. Joubert, A. Salameh, V. Krakoviack, F. Delbecq, P. Sautet, C. Copéret, J. M. Basset, *J. Phys. Chem. B* **2006**, *110*, 23944–23950.
- [17] C. Thieuleux, E. A. Quadrelli, J. M. Basset, J. Döbler, J. Sauer, *Chem. Commun.* **2004**, *4*, 1729–1731.
- [18] G. L. Casty, M. G. Matturro, G. R. Myers, R. P. Reynolds, R. B. Hall, *Organometallics* **2001**, *20*, 2246–2249.